2003

Spectroscopy with surface plasmons

Mondona Renee Zangeneh
San Jose State University

SPECTROSCOPY WITH SURFACE PLASMONS

A Thesis

Presented to

The Faculty of the Department of Chemistry

San Jose State University

In Partial Fulfillment

of the Requirements for the Degree

Master of Science

by

Mondona Renee Zangeneh

August 2003

INFORMATION TO USERS

The quality of this reproduction is dependent upon the quality of the copy submitted. Broken or indistinct print, colored or poor quality illustrations and photographs, print bleed-through, substandard margins, and improper alignment can adversely affect reproduction.

In the unlikely event that the author did not send a complete manuscript and there are missing pages, these will be noted. Also, if unauthorized copyright material had to be removed, a note will indicate the deletion.

ProQuest Information and Learning Company
300 North Zeeb Road
P.O. Box 1346
Ann Arbor, MI 48106-1346

APPROVED FOR THE DEPARTMENT OF CHEMISTRY

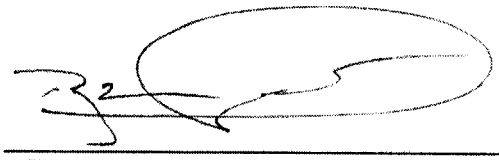

Dr. Roger H. Terrill

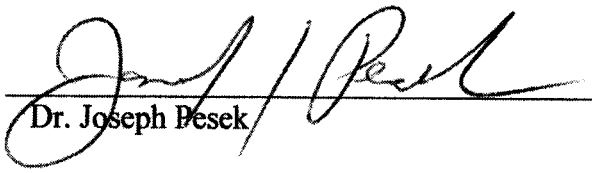

Dr. Joseph Pesek

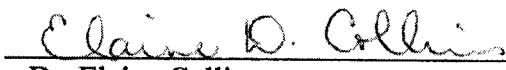

Dr. Elaine Collins

APPROVED FOR THE UNIVERSITY

ABSTRACT

SPECTROSCOPY WITH SURFACE PLASMONS

by Mondona R. Zangeneh

A highly sensitive technique such as surface plasmon resonance (SPR) spectroscopy has become a widely used optical sensor for probing biochemical interactions. This sensor is capable of monitoring dynamic processes in real time and providing useful kinetic and thermodynamic information.

A novel instrumental method for angle and wavelength modulated surface plasmon resonance (SPR) spectroscopy is applied to the problem of spectral selectivity in SPR experiments. For transparent analytes, SPR reflectivity data are reduced to a 2-D spectrum of resonance wavelength versus incident angle – $\lambda_{SPR}(\theta)$. This spectrum encodes the RI dispersion of the analyte and illustrates the increased SPR spectral shift per unit RI change at longer wavelengths (lower angle). For the absorbing analyte magnesium phthalocyanine (MgPc), the 2-D data reduction method is complicated by the way the SPR and MgPc-based spectral peaks mix. Fresnel reflectivity models support experimental observations of spectral branching and qualitative fingerprints in the form of branched spectra and difference reflectivity $\Delta R(\lambda,\theta)$ contour plots are presented.

ACKNOWLEDGEMENTS

I first want to thank Dr. Roger Terrill for allowing me to join his group. I have learned so much and am grateful for the wonderful opportunity. He provided a comfortable environment and has been very patient with my many questions. He has truly been an excellent mentor.

I appreciate the comments on my thesis provided by my research committee, Dr. Pesek and Dr. Collins, as well as their time spent on my seminars and oral exams.

I would like to thank all of the faculty members of the Chemistry Department for the support and kindness they have shown.

I would like to thank all the students in the Chemistry department for their friendship. Also, I want to thank the research students in my laboratory group for their support.

Last, but certainly not least, I would like to thank my family. I would like to thank my mother for encouraging me to always put education first. I would like to thank my grandma, aunt, and uncles for all their support. I also would like to thank my sister for her funny jokes because I could sure use some laughter. The love my family has provided is what has allowed me to succeed.

TABLE OF CONTENTS

LIST OF FIGURES

1.0 Introduction

Surface Plasmon Resonance Spectroscopy (SPRS) is a sensitive optical technique that detects changes in refractive index of analytes near a metal surface. SPRS monitors chemical, physical, and biochemical processes at metal interfaces *in situ*. It is a method that is cheaper and simpler than ellipsometry or fluorescence. Also, it is robust, stable, and has good spatial resolution (~10 microns). As early as 1902, R.W. Wood observed that excitation of surface plasmons was the cause of anomalous diffraction on diffraction gratings. By the late sixties, Kretschmann and Otto investigated optical excitation of surface plasmons. In the seventies, Pockrand and Swalen used SPRS to characterize thin films and J.G. Gordon used SPRS to monitor metal interfaces. Then, in 1982, Nylander and Liedberg used SPRS for gas detection and biosensing (1).

Since that time, SPRS has gained popularity in the biochemical field for the many advantages it has to offer. The use of SPRS in the biochemical field is advantageous in that dynamic processes can be monitored in real time within seconds without the use of labeled molecules. For example, SPRS is faster than using techniques such as enzyme-linked immunoassays (ELISA), and may yield more information such as association and dissociation kinetics, and binding constants (2).

Commercialization of SPRS by BIAcore (originally Pharmacia Biosensor AB) was established in 1990. Texas Instruments has also introduced an optical biosensor called Spreeta. Both of these companies utilize angular interrogation and prism couplers. Quantech has offered biosensors utilizing grating based structures and wavelength

interrogation. Also, multimode optical fiber waveguide based sensors that EBI sensors have developed use wavelength interrogation. BIAcore has acquired EBI sensors (1).

SPRS simply involves using a light source to analyze metal/dielectric interfaces. In the most widely used configuration, dubbed the "*Kretschmann configuration*" (3), the light is totally internally reflected (TIR) off of the interface between a prism and a 50nm metal film. In this TIR setting, the electric field of the reflecting light penetrates slightly into the metal film and the optically rare medium on the outside of the interface (see **Figure 1**). This penetrating electric field is described as an evanescent wave because the field strength decays strongly with distance away from the reflecting interface. Under appropriate conditions, surface plasmons (also known as plasmon surface polaritons) are excited in the metal film surface that is in contact with the solution. Surface plasmons can be described as collective oscillations in the free electron gas on the surface of the thin metal film (about 50nm). In SPR, these oscillations are driven by the evanescent electric field of light totally reflecting at a glass | Au (50 nm) interface (4). This resonant excitation of plasma oscillations results in a sharp attenuation of the reflected light at a certain combination of wavelength and angle. In the seldom-used Otto configuration (4), a very thin air gap is used to couple the evanescent light with the surface of bulk gold in a format where there is glass | air ($\leq$ 500nm) | Au. In the Kretschmann configuration, the sensitivity of the SPRS method decreases exponentially with distance away from the metal surface, roughly in proportion to the electric field strength of the evanescent wave as it penetrates into the analyte solution contacting the Au film. The effective penetration depth is about 500 nm for visible wavelength experiments.

Figure 1. Attenuated total reflection geometry for the excitation of surface plasmons. **A.** Upper left figure shows optic with Au film and solution layers. Expanded view of interface depicts the interaction of the electric field component of a light wave incident at angle theta and projecting a transverse electric field component onto the Au surface with a period of λ". **B.** Calculated surface plasmon resonance absorption bands as a function of incident angle (left) and as a function of wavelength (right). Pairs of curves reflect the response of the band position for both a bare (left curves) and a coated Au surface (right curves).

Figure 1. SPR spectroscopy in the Kretschmann configuration

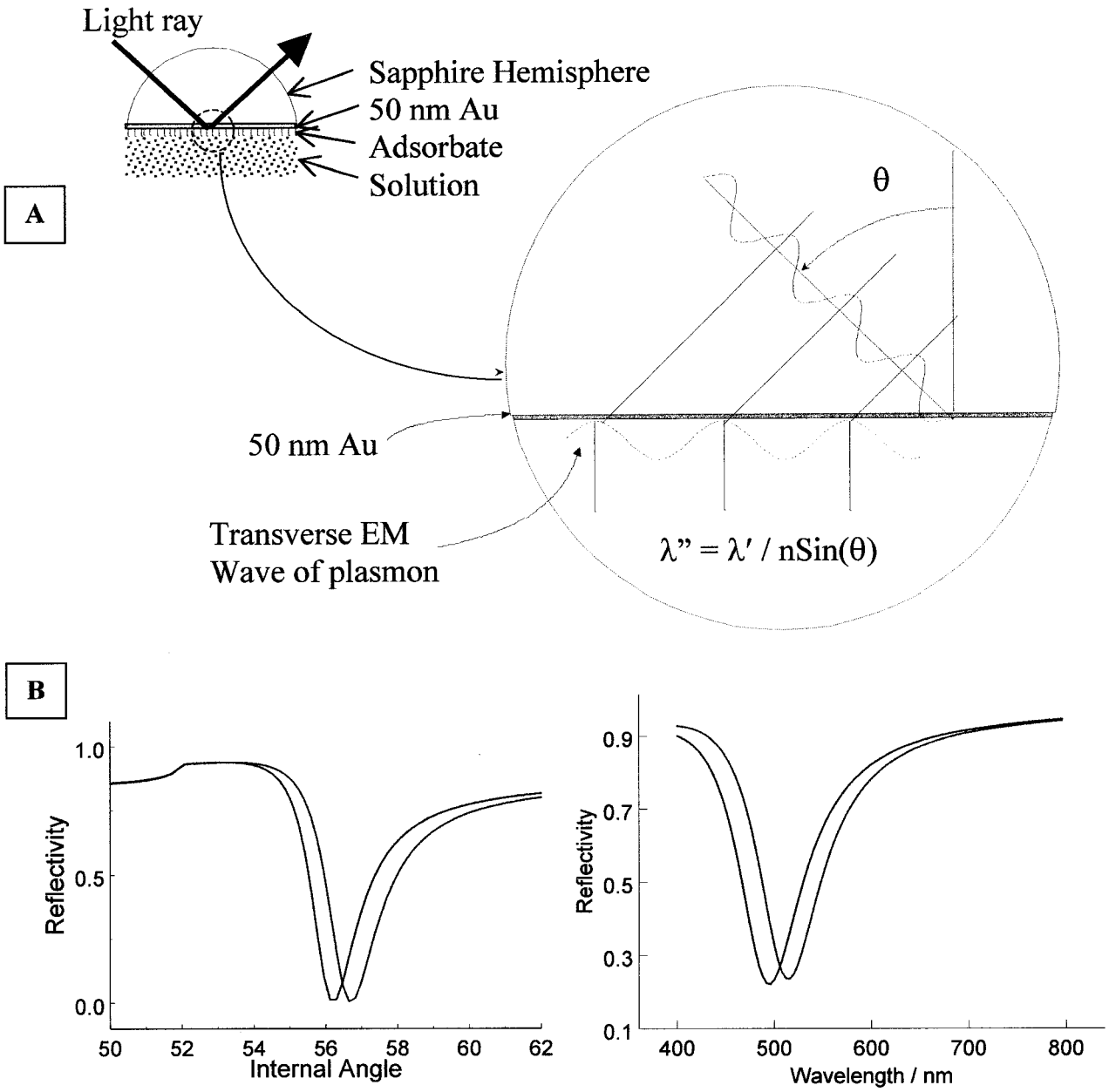

In the Kretschmann configuration, the excitation of surface plasmons occurs when the component of the wave vector of the incident light that is parallel to the interface equals that of the surface plasmon. The component of the wave vector of the incident light that lies in the surface plane is given by (4):

1. $$k = \frac{2\pi}{\lambda o} n_p \sin(\theta)$$

Where:

λo = the vacuum wavelength of the light

n_P = the prism refractive index and

θ = the angle of incidence of the light

The approximate wave vector of the surface plasmon is given approximately by:

2. $$k_{SP} = \frac{2\pi}{\lambda o}\left(\frac{\varepsilon_M \varepsilon_S}{\varepsilon_M + \varepsilon_S}\right)^{1/2}$$

Where:

ε_M = the complex dielectric constant of the metal and

ε_S = the dielectric constant of the solution layer

Thus, excitation of surface plasmons occurs for the specific combination of λ, θ, n_P, ε_M and ε_S etc. such that $k = k_{SP}$, and therefore Equation **1** equals Equation **2**.

If more exact comparisons between experiment and theory are desired, the Fresnel equations may be employed. This is the method that we employ exclusively in our studies.

Thin metal films used in SPRS have included gold, silver, and copper (2). The average thickness of a metal film used in SPRS studies is ~50nm. The variety of metals that can be used for SPRS is limited by the complex dielectric constant of the metal, ε_M because this in part determines the wave vector of the surface plasmon (4). The most common metal used in SPRS has been gold due to its stability. Vapor deposition and sputtering are the most common ways of producing SPR active metal films (1).

Silver has also been used in studies due to the sharp resonance peak observed, however silver can be problematic in that it more easily corrodes than does Au (2). There has been some effort in using silver surfaces for SPRS studies by analyzing modifications of silver. Zhu et al. (5) are an example of a group that have found ways to modify silver so that silver would become inert and thus made practical for use in SPRS studies. Oxide coated silver films were treated with chemicals and heated. Some oxide coated silver films may have use in robot-printed DNA arrays and in situ DNA synthesis. Both are important in high-throughput sensor applications.

Although SPRS has opened up many opportunities for the biochemical field, there is still a need for improvements. Homola et al. (1) have provided suggestions in their review paper for improving SPRS. First, they state that detection limits need to be improved. Second, improving multichannel performances for use in pharmaceuticals is suggested. Berger has contributed to the first steps developing multichannel SPR sensors. Since their review, Homola et al. have presented a sensor configuration for multichannel performance that helps to distinguish nonspecific responses, such as those due to temperature drift and changes in the bulk refractive index of a flowing buffer from

analyte-based ones. For example, Lu et al. (6) have used multichannel SPR for protein array detection. Cross-interference among adjacent areas was accomplished by placing an overlayer of tantalum pentoxide on part of the gold surface. This overlayer spectrally shifts the SP resonance at that point on the sensor to longer wavelengths. The SPR-Ta signal then serves as a reference channel that can detect changes in bulk solution refractive index changes and has no binding sites.

Developing selectivity in SPR sensing is a central theme of this thesis. As proposed to that idea, Homola et al. discuss how SPRS is a nonselective platform, and that other techniques would need to be coupled to SPRS in order to distinguish nonspecific binding. The premier example of methods that can be coupled to SPRS for the purpose of identifying adsorbates is matrix-assisted laser desorption/ionization time-of-flight mass spectrometry (MALDI-TOF/MS) (7,8). However, MALDI-TOF/MS is an expensive technique. In most cases, selectivity in SPRS methods is purely a function of analyte selectivity of surface-attached ligands (9). However, this may not be enough if mixtures are to be analyzed. If a SPRS method with inherent spectral selectivity could be developed, then this would reduce the need for other costly techniques.

2.0 Research Goal

The major goal of this project is to develop an experimental mode of SPRS that has the quality of spectral selectivity. The lack of selectivity in SPRS was noted in the literature. Karlsen et al. (10) refer to conventional SPR sensors as 'zeroth-order' ones because they reduce the entire reflectivity spectrum to a single datum – namely θ_{SPR} or λ_{SPR} – the angle or wavelength corresponding to maximum resonance absorption. In the experiments described below, we have endeavored to impart spectral selectivity in our SPRS method by acquiring SPR data in an expanded data set that measures reflectivity as a function of both angle and wavelength. In doing so we developed a 'first-order' SPR sensor that produces a spectral response that reflects the wavelength dispersion in the refractive index of the analyte. This spectral response is potentially useful as a distinctive 'fingerprint' for a given analyte and thereby imparts a degree of selectivity to the otherwise generic SPR sensor.

Transparent analytes (acetone, acetonitrile, and isopropanol) and an absorbing dye molecule (magnesium phthalocyanine) were investigated with our first order SPRS method and spectral responses characteristic of the RI dispersion of these analytes are presented.

We found that transparent analytes, such as acetone, exhibited only subtle, i.e. normal, dispersion in refractive index and this dispersion proved insufficient for distinguishing different analytes of similar refractive index. So an appropriate analyte, magnesium phthalocyanine (MgPc), was employed that exhibited a strong anomalous dispersion (a characteristic oscillation in refractive index that accompanies an absorption

band). The resulting SPR experiments clearly reflected the visible absorption spectrum of MgPc.

Because anomalous dispersion is needed, the selectivity of our SPR method is coupled to light absorption. But the great majority of interesting SPR analytes, i.e., proteins etc., are transparent to visible light. This implies an eventual change to either higher or lower frequency measurements. Again, the major focus of these studies is to develop a SPRS method that augments the quantitative SPR response with qualitative spectral information.

3.0 Optical Configurations for SPRS

Various configurations have been explored to couple light with surface plasmons for use in SPR sensors. These have included prism-coupling, waveguide coupling and grating coupling. **Figure 2** shows diagrams of each configuration. Arrows represent the ray of incident light and reflected or diffracted light.

3.1 Prism-coupler based (ATR method)

The prism-coupler method is either in the Kretschmann (ATR method) or Otto configuration (4). Most studies have utilized the Kretschmann configuration. The base of a prism is coated with ~50nm of gold. All the main detection methods (angle shift, wavelength shift, imaging) have been used. This system provides flexibility in the choice of the analyte, high-resolution measurements and the development of multichannel SPR-sensing devices are possible (1).

3.2 Optical waveguide

This configuration has been used for the benefits of small size, ruggedness and the ability to suppress stray light. All the main detection methods have been used with this system. For optical fibers the cladding is removed and a thin silver film is deposited on the fiber core. Jorgenson and Yee first used optical fibers with the wavelength interrogation technique. This method allows the highest level of miniaturization of all the SPR devices (1). A new type of waveguiding system consists of a light pipe that is a glass slide containing a gold sensing layer on one surface (11).

3.3 Grating-coupler based

The grating coupler is useful in settings where it is advantageous to use an external reflection light reflection. For example, by depositing a gold grating onto the surface of a quartz crystal microbalance one can simultaneously measure the optical and mass response of an adsorbing system (12). It is also convenient that the thickness of the Au or Ag layer is not critical for grating coupling as it is the for ATR (Kretshmann) coupling. When coupled by an Au or Ag grating the surface plasmon is evident as anomalies in the normal diffraction pattern. The anomalous diffraction can be detected as a function of either wavelength (for broadband illumination) or angle (for monochromatic illumination). A disadvantage of this system is that the analyte and flow cell need to be optically transparent since the incident light beam is through the sample solution (1).

Figure 2. The three general SPRS configurations. A. Prism-coupler. B. Waveguide-coupler. C. Grating-coupler. Of these configurations, the prism-coupler is most widely used. Our experiments utilize this configuration.

Figure 2. General SPRS configurations

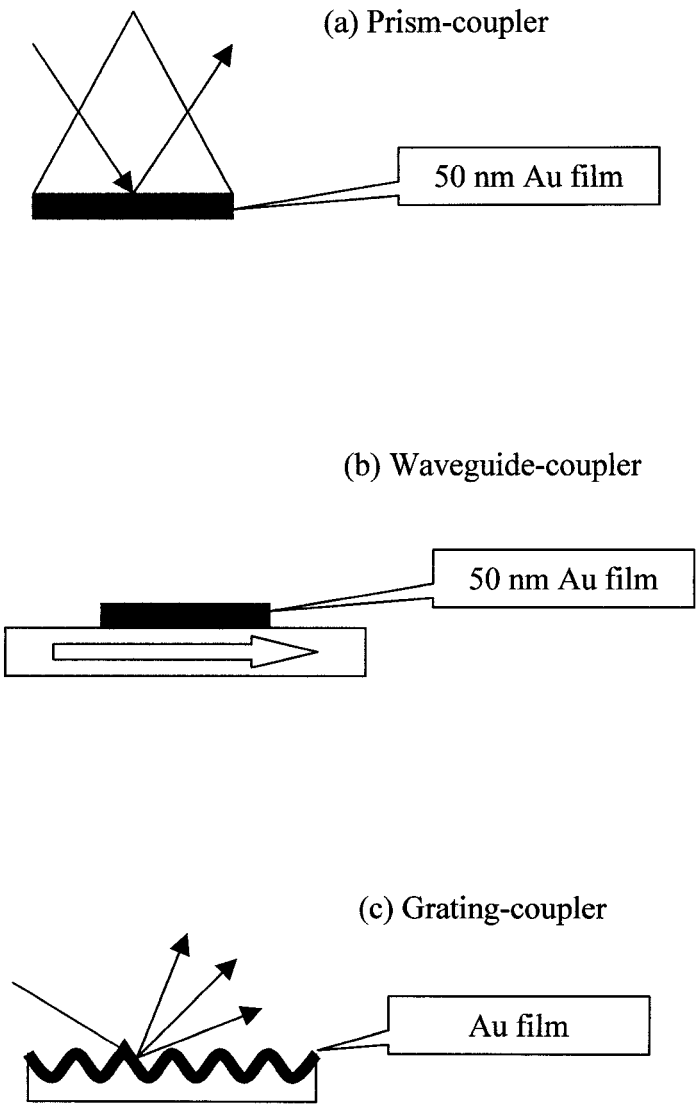

4.0 SPR Spectroscopic Modulation Modes

SPR data may be collected in various ways – commonly referred to in the literature as "modulation modes." The three most common ways are to measure changes in reflected light intensity (often used for imaging), changes in SP coupling wavelength, and changes in SP coupling angle. More recently, optical phase change upon reflection has been exploited as well in a hybrid Ellipsometry-SPR measurement.

4.1 Angle modulation (scanning angle SPR)

This is the most common method used in the SPRS optical biosensor. At a fixed wavelength, reflectivity is measured as a function of angle $R(\theta)$. An angular shift in the location of the surface plasmon absorption, θ_{SPR}, will result from changes in refractive index. In this mode, one typically scans the beam through a range of angles and monitors the reflected light for the precise angle of the reflectivity minimum. This can also be accomplished by focusing light on the sample, and monitoring the divergent reflected beam for a dark band that will move according to the SPR coupling angle. A single wavelength (often HeNe laser, 632.8 nm) excitation source is often used for angle modulation experiments. Paired red and green HeNe laser lines at 632.8 and 543.5nm are useful for obtaining interfacial parameters using this SPRS mode (11). Diode lasers, light emitting diodes and near IR lasers have been used as well (9).

4.2 Wavelength modulation (wavelength shift)

To use the wavelength at which the SPR is coupled (λ_{SPR}) for analysis one employs a fixed angle and a well-collimated beam of white light. The reflected light spectrum, $R(\lambda)$, then contains an absorption peak at λ_{SPR}. Shifts in λ_{SPR} occur when adsorption of material is detected at the interface. The 600 to 800 nm wavelength range is often used for these measurements (9).

4.3 SPR Imaging

Earlier work done with polymers at the Max Planck Institute referred to this mode as SPR microscopy (13). A collimated monochromatic light beam is used for illumination of the sample at a single incident angle, near the SPR angle, and light is reflected from the surface and collected onto a CCD array detector. The CCD thus records a monochrome reflected light image of the surface. For a given monochromatic light source the incident angle is tuned so that $dR/d\theta$ is maximized. At this angle, slight changes in near surface refractive index result in large changes in reflected light intensity. Intensity in these images is then proportional to near surface refractive index. In this configuration, the laser source is sometimes replaced with a collimated white light source and a narrow-band near IR interference filter. This combination is superior to the more common HeNe based one because NIR wavelengths exhibit larger $dR/d\theta$ (i.e. a sharper SPR resonance) and interfering laser speckle and interference fringes are absent. SPR imaging can be used to monitor binding of analytes to arrays of probe molecules in a "genechip" format (9).

4.4 Phase Modulation

In this SPR mode, the phase change of the p-polarized light reflection is measured in the vicinity of the SPR angle using an ellipsometer (14). The relationship between the sample refractive index and the phase can be modeled using the Fresnel equations. A sensor based on phase modulation is up to three times more sensitive than one based on angle or wavelength modulation, but does not have as broad a dynamic range (15) because phase changes repeat every 360 degrees.

5.0 Quantitative Analysis of SPRS Data

5.1 Calibration curves

Jung et al. (16) have provided a simple method of extracting quantitative measurements of either the thickness or surface concentrations of an adsorbed layer from a SPR sensor. They discuss how previous researchers have obtained quantitative measurements of adsorbate film thickness and coverage from a calibration curve of response versus thickness or surface concentration. Sjolander et al. and commercial instruments, BIAcore use this type of linear calibration curve (17). However, this calibration is limited to studying the same adsorbate or adsorbates with similar dielectric properties. They indicate that responses to thicker (i.e., $d \geq 300$ nm) films have been studied, but that the calibration curves are nonlinear. The SPR response is a linear function of bulk refractive index as well. Other authors have presented methods of determining thickness, surface concentration or fractional coverage from measured SPR responses (16).

5.2 Multiparameter analysis

There has been some debate regarding the feasibility of measuring more than one interfacial parameter using the SPR response. Peterlinz et al. have proposed a two-color SPR spectroscopic method to determine both parameters unambiguously. In this two-color approach, He-Ne laser sources at 632.8 nm (red) and 543.5 nm (green) are both employed and the n and d from simultaneous curve fits (18,19) appear to avoid ambiguity. Some controversy remains however in this area. For example, Ehler et al. (20) argue that the two-color approach is only suitable for colored overlayers. Chinowsky and Yee presented mathematical methods of linear estimation to analyze the two-color SPR technique proposed by Peterlinz and Georgiadis. Their results indicate that while refractive index and thickness of the film can be estimated from a SPR reflection spectrum, they do so with a somewhat large uncertainty (21).

5.3 Kinetics

SPRS provides kinetic information for studying binding and releasing events because SPR data can be collected fairly rapidly ($\tau \geq 0.1$s). Peterlinz and Georgiadis were among the first to demonstrate this. They used SPRS to monitor organic thin film growth of self-assembled monolayer (SAM) films of n-alkanethiols on gold (19). Film thickness versus time was monitored. SPRS data are also used for measuring adsorption, desorption and diffusion kinetics in DNA hybridization experiments (22).

5.4 Thermodynamics

Thermodynamic information can be obtained from quantitative SPRS results. Peterson et al. showed perfectly matched DNA probe-target experiments exhibit 100% hybridization, fast kinetics and can be modeled with a Langmuir isotherm. On the other hand, mismatched targets did not reach 100% hybridization and were better modeled with a complex heterogeneous model called a SIPS isotherm:

3. $$\Gamma = \Gamma_{MAX} \frac{(K_A C)^a}{1 + (K_A C)^a}$$

Where: K_A = k_{ON} / k_{OFF}

C = Solution concentration of adsorbate

Γ = Surface coverage of adsorbate

Γ_{MAX} = Maximum surface coverage adsorbate

The SIPS model above corresponds to the Langmuir isotherm when a=1 (23).

6.0 SPRS Combined with Other Analytical Techniques

Other analytical techniques that have been combined with SPRS have included the following: Quartz Microbalance (QCM), electrochemistry, fluorescence, ellipsometry, interferometry, surface enhanced Raman spectroscopy (SERS) and matrix-assisted laser desorption ionization mass spectrometry (MALDI-TOF/MS).

6.1 SPRS and QCM

While SPRS is sensitive to the optical properties of an adsorbed film, QCM measures the frequency change of a quartz crystal oscillator resulting from the mass and viscoelastic properties of material adsorbed to the sensor surface. For example, Bailey et al. used this combined technique for monitoring the solution phase adsorption of the perfluoropolyether lubricant Fomblin ZDOL onto a silver surface. From the two techniques they were able to obtain information on the actual density, refractive index and conformation of ZDOL molecules at the solid-liquid interface (12).

6.2 SPRS and electrochemistry

Many groups have utilized this combination. The gold thin film on the substrate is used as both a medium for surface plasmons and the working electrode for electrochemical analysis. Brennan et al. (24) have studied prussian blue films using a fiber optic based SPR instrument with electrochemistry. Reduction of prussian blue to prussian white resulted in a refractive index change detected by SPRS. Iwasaki et al. (25) have used a prism based SPR instrument using a multienzyme layer modified electrode to study SPR detection of enzymatic reactions and measurements of glucose concentration. The chemical conversion of an enzymatic reaction to a dielectric property change was obtained. This combination holds promise in investigating different enzymes on one electrode. Baba et al. (26) have used SPRS and light scattering with electrochemistry to study the optical and electrochemical properties of polyaniline films on a planar gold

electrode. SPRS kinetic reflectivity curves with cyclic voltammograms were used to understand the properties of these conducting polymers. Kang et al. (27) combined cyclic voltammetry and SPRS for studies of polyaniline growth and properties of the film. Angular scans illustrated curves that shifted to higher angles as the polyaniline film thickened. The switch between the oxidized and reduced states of polyaniline caused large changes in reflectivity. Boussad et al. (28) present a multiwavelength SPR technique for measuring electronic states of the molecules used for identification purposes. Cytochrome C was immobilized on a modified gold electrode and examined in order to understand the electronic and conformational differences between the redox states. Changes in the resonance angle due to conformational changes were detected as a result of the oxidized and reduced states of cytochrome C.

Many other groups have utilized this combination. An electrochemical process such as adsorption of species or modification of the electrode surface can affect the excitation of surface plasmons. Thus, SPRS is shown to be sensitive to the nature of an electrochemical interface.

6.3 SPRS and fluorescence (SPEF)

This combination, coined surface plasmon enhanced fluorescence (SPEF) by Roy et al., was used to probe the enzyme kinetic interaction with a substrate surface. The molecule on the gold modified surface absorbs energy from the plasmons and emits light that is detected by a photomultiplier tube detector that is positioned below the optic. The SPEF signal rises after addition of labeled protein. The SPR signal rises when both

unlabeled and labeled avidin is added to a monolayer of biotin. These two signals can then be used for separating labeleled and unlabeled species. This combined technique may be advantageous for detection of multiple species (29).

6.4 SPRS and ellipsometry (SPEE)

Westphal and Bornmann have combined these two techniques calling it surface plasmon enhanced ellipsometry (SPEE). In ellipsometry, circularly polarized light is reflected from a sample surface. The presence of adsorbates generally retards the phase or intensity of the P or the S components of the light and this is evident in the ellipticity of the reflected light. By making ellipsometric measurements under conditions where surface plasmons are excited simply enhances the sensitivity of the ellipsometric measurement. The sensitivity of this combined technique is reportedly enough for detecting changes in thicknesses of biomolecular layers less than 10 pm. With the SPEE setup, a hybridization experiment involving biotinylated DNA strands was performed. The DNA hybridization was clearly detected, so this method is suggested for use with DNA microarrays (30). Optical phase detection has a limited dynamic range however because the phase values repeat every 360°.

6.5 SPRS and interferometry (SPRI)

Nikitin et al. have combined SPR and interferometry in a clever experiment dubbed SPRI (31). In this mode, the interrogating beam is split and directed into two matched interferometer arms. One arm has a reference mirror and the other the SPR

sensor surface in the Kreschmann configuration. The beams are then recombined and collected on an imaging, e.g. CCD detector. In this setting, differential phase retardation at the SPR sensor surface contributes to intensity contrast at the detector. This mode is more sensitive than most SPR sensor modes, but has a limited dynamic range, again because phase changes repeat on 360° intervals.

6.6 SPRS and SERS

It is well known that Raman signals can be strongly enhanced when the excitation energy is coupled into the scattering molecules through the localized surface plasmons that propagate in roughened silver metal surfaces. But surface plasmons can also be coupled to Raman scatterers on the metal surface in both Kretschmann and grating configurations. Nikitin et al. recently exploited Raman scattering originating from molecules on an SPR sensor surface in a sensing format. In this experiment a gold film was deposited on the surface of a Si grating. The resulting sensor produced both SPR absorption and an enhanced Raman scattering response. The aggregate response was useful for the detection of ppm concentrations of NO_2 that coordinated to adsorbed phthalocyanines (32).

6.7 SPR-BIA and MALDI-TOF/MS (BIA/MS)

This combination was coined BIA/MS by Nelson et al. (7). In these experiments, Matrix-assisted laser desorption/ionization time-of-flight mass spectrometry (MALDI-TOF/MS) is used to interrogate SPR sensor surfaces *ex-situ* following a specific binding

event detected by SPR. The MALDI-TOF/MS provides qualitative information and therefore affords selectivity to SPR. For example, MALDI-TOF/MS can be used for identification of proteins, and the analysis of their post-translational modifications. Importantly, the MALDI-TOF/MS step can identify non-specific binding. SPR-BIA is often used for isolating proteins from solution by exploiting the affinity of solution targets to probe molecules covalently anchored to the SPR sensor surface. This is sometimes referred to as planar geometry affinity chromatography. In SPR-BIA, SPR is used for detection and quantitation of binding and then MS is used for qualitative analysis of the bound material. For example, detection of attomole amounts of beta-2-microglobulin captured from urine by BIA/MS has been demonstrated (7,8). Importantly, the resolution of the TOF/MS step allows for the parallel detection of multiple biomolecule targets.

7.0 Nanoparticle based SPRS

An alternative strategy for development of optical biosensors is based on noble metal nanoparticles. One of the most successful examples employs triangular silver nanoparticles on surfaces. This method was pioneered by Van Duyne and coworkers and was termed "localized surface plasmon resonance spectroscopy" or LSPR (33, 34). These triangular nanoparticles are deposited onto a glass surface by vacuum deposition through a periodic mask made by an adsorbed layer of polystyrene microspheres. Following metal deposition, the polystyrene spheres are rinsed away and the roughly triangular interstitial spaces between the spheres result in metal "nanotriangles" arrayed

on the substrate surface. The optical properties of the triangles are such that light at normal incidence to the surface can excite surface plasmon modes in them referred to as localized surface plasmons. Thus, the nanoparticle arrays can be interrogated in a simple transmission geometry. The resonant frequency of a given LSPR mode depends on factors such as the size, shape, dielectric properties and local environment of the nanoparticle. In a typical LSPR measurement, an LSPR sensor is interrogated with broadband light and shifts in the wavelength absorbed by the LSPR mode reflect changes in near-surface refractive index analogously to wavelength modulated SPR sensors. LSPR sensors based on triangular nanoparticles were shown by Van Duyne et al. to be less sensitive to changes in bulk refractive index than comparable planar SPR sensors with little compromise in near surface sensitivity. This property is important because in most SPR sensing configurations, bulk refractive index changes are a serious source of unwanted background signal.

8.0 Applications of SPRS

Areas of SPRS applications include thin film metrology, chemical and biosensing.

8.1 Metrology

SPRS has been used to the analysis of thin films such as organic self-assembled monolayers, Langmuir-Blodgett and polymeric layers. Thickness, optical frequency dielectric properties, adsorption processes, surface degradation and hydration information has been obtained (2).

8.2 Chemical

Most chemical SPR sensors are based on measurement of SPR variations due to adsorption directly to the metal surface or to a chemical reaction of an analyte with a transducing medium. Nylander and Liedberg first used SPRS in 1982 for gas detection. A film of silicon-glycol copolymer was exposed to different concentrations of the anaesthetic gas, halothane and measured by SPRS. Other groups have monitored the concentration of vapors of aldehydes, alcohols and detection of NO_2, H_2S and NH_3 vapors with SPRS (1). Ion sensors utilizing SPR have also been investigated using adsorbed chromoionophores, molecules that change their color on complexation with the compound that is to be measured. The chromoionophore that was used consisted of a merocyanin dye coupled to a metal-complesing crown moiety (35).

8.3 Biosensing

Most of SPR applications are devoted to biosensing. Early work focused mainly on antigen-antibody interactions, streptavidin-biotin reactions and some IgG examinations for development of SPRS setups (36,37). Advanced systems have examined protein-protein or protein-DNA interactions and conformational changes in an immobilized protein. Other biochemical systems have been examined and other interests for future biosensing involve quantification of T cell receptors with ligands of interest (1).

The general method of antibody immobilization for SPRS applications is the use of a carboxymethyldextran matrix bound to a gold substrate. Treatment of the dextran

layer with iodoacetic acid results in carboxylic groups. The use of this hydrophilic layer is advantageous because it increases SPRS sensitivity, prevents nonspecific protein adsorption and the surface can be regenerated and reused. Coupling of a ligand with a functional group such as NH_2 is done by treatment of the carboxylic groups with N-hydroxy succinimide (NHS) and ethyl-methyl-diaminopropyl-carbodiimide (EDC). A dextran layer containing streptavidine molecules can also be used for binding biotinylated ligands (1).

Alkanethiols can chemisorb on gold and silver surfaces to form self-assembled monolayers (SAM's). The use of SAM's of thiol molecules is for connecting biological substituents as tail groups on the surface of the metal film (1). Spinke et al. (38) demonstrated the use of SAM's for a streptavidin/biotin binding system. With this system, the binding interaction of a biotinylated thiol gold surface and streptavidin allowed for immobilization of biotin-labeled protein. Another example shown by Sigal et al. (39) utilized SAM's to selectivity bind to a protein whose primary sequence terminates with a histidine tagged protein. The gold surface was prepared in a similar manner as nickel-affinity chromatography that is a procedure used for purifying histidine tagged proteins. The gold surface was modified with a mixture of two alkanethiols. One thiol terminated with a nitriloacetic acid (NTA) group that formed a chelate with Ni(II). The second thiol was terminated with a tri (ethylene glycol) group that resisted protein adsorption. The interest for this method of immobilization of proteins is for control of the protein's orientation so that its active site can interact with molecules in solution. Also, this specific immobilized protein would be able to resist nonspecific binding of other

proteins. The use of SAM's formed on gold substrates instead of silver is mostly utilized because silver ions can be toxic to living cells (2). There has been interest in using SAM's for investigating the interaction of cells with surfaces in vitro and sensing mechanisms of cells (40).

9.0 Practical Aspects of Our Experiments

9.1 Background

Transparent analytes (acetone, acetonitrile, and isopropanol) and an absorbing dye molecule (magnesium phthalocyanine) have been investigated with SPRS utilizing a simultaneous multiangle and multiwavelength scanning capability in our group with the aim of using using SPRS for measuring RI dispersion and eventually molecular fingerprinting. Instrument design and instrumental aspects related to this goal are detailed below. The rationale for this approach is discussed more extensively in subsequent sections.

9.2 Materials

Isopropanol, acetone, acetonitrile, and toluene (HPLC grade, Fischer) and water (Millipore) were used as solvents throughout the experiment. Magnesium phthalocyanine (MgPc) was purchased from Aldrich and used as received. Au for evaporation was 99.99% pure (Canadian Maple Leaf), and Cr (99.9%) was obtained from Alfa-Aesar. Visible absorbance spectrum of MgPc was recorded on a Cary 50 instrument

for the purpose of calculating the optical constants of the solutions for use in Fresnel simulations of the SPR reflectance spectra.

9.3 Thin Film Preparation

A hemispherical sapphire optic (Harrick Scientific) was used as a substrate for Au films used in this study. Prior to deposition of metals the optic was cleaned with chromic acid in concentrated sulfuric acid followed by deionized water and isopropanol rinses. Coatings of 1nm of chromium and 50nm of gold (Maxtek TM100) were vapor deposited at a pressure of approximately $5x10^{-6}$ Torr. Following deposition, Au films were annealed in the evaporator for 30 minutes at approximately 200°C. This treatment was observed to reduce the bandwidth of the SP resonance.

9.4 Instrument Design

A custom designed surface plasmon spectroscopy apparatus was constructed for these studies based on a modified Harrick Scientific Seagull® variable angle reflection accessory and an Ocean Optics S2000 CCD based fiber optic spectrometer and tungsten halogen light source. Light is collected into a 400-micron optical fiber, transmitted to the Seagull®, polarized and stopped down to approximately f/64 using either a slit or a pinhole before being directed toward the optic. The Seagull® provides a variable angle-of-incidence reflection spectrum of the sapphire-Au film interface. The variable angle system uses a pair of elliptical mirrors that share a focus at the center of the hemispherical optic, and a pair of tilting mirrors located at the two opposite foci. This

design is one in which the incident light is focused at the center of a hemispherical optic. This "center focus" design allows for angle adjustments to take place without changing the focal point (i.e. the sapphire prism) and eliminates chromatic aberrations but at a slight cost in angle resolution. Angle resolution of about 0.5° is achieved by constraining the range of incident angles with a horizontal slit. A stepper motor provides control over the angle of incidence with high resolution and repeatability. The output of the fiber optic is coupled to the 2048 channel S2000 spectrometer providing rapid spectral acquisition at 0.25nm instrumental resolution. A stainless steel flow cell is coupled to the optic with a Kalrez® O-ring. Static nitrogen pressure drives solutions through a computer controlled, zero dead volume, all PTFE 6 port-switching valve into the cell. PFA tubing of 1/16" bore is used throughout. Ozone generated with a Hg pen-lamp (UVP, Inc.) in flowing O_2 is used periodically to clean the Au surface.

9.5 Data Acquisition

Computer control of flow, polarization, angle of incidence and spectral data acquisition and analysis is achieved using programs written in National Instruments LabView®. Determination of the SPR coupling angle is achieved in real time by fitting a polynomial to the spectral peak. For acquisition of reflectivity surfaces, TM (P) polarized reflection spectra were acquired typically over a 5° interval at 0.1° resolution. The spectral power reference data are acquired when dry N_2 is present in the cell instead of solution so that the plasma resonance is absent but all other reflections are identical. This method proved much more satisfactory than employing the S-polarized reflectance

presumably due to unaccounted-for polarization dependence in optical components such as the spectrometer.

9.6 Fresnel Simulations

Fresnel reflectivity calculations of a 4-layer system were derived from a paper by Bohn (41), and entered into a Mathcad 2001® worksheet. Simulations employ the wavelength dependent optical constants ($n(\lambda)$ and $k(\lambda)$) of sapphire, gold and MgPc. Simulations of the Au-SPR peak that included the Cr-adhesion layer exhibited slightly broader resonance peaks but were otherwise nearly identical, so Cr was ignored for 4-layer calculations based on the following strata:

Sapphire | Au(50nm) | MgPc(1nm) | acetone.

9.7 Detailed Experimental Procedures and Data Acquisition with Labview Software

Before a SPR spectrum is taken it is necessary to have a clean gold film present on the optic. This is accomplished by cleaning the Au film with ozone followed by N_2 and then a pure isopropanol rinse and another N_2 purge for drying the cell.

Before running any samples through the flow cell, it is important to see if coupling between the incident incoming light and the plasmons in the metal takes place (resonance). This is accomplished with a LabView® program interfaced to an Ocean Optics S2000 CCD spectrometer. A surface plasmon resonance band is evident as a well-defined curve is displayed in a reflectivity versus wavelength graph as seen in **Figure 3**. One can also monitor the wavelength of the SPR absorption in real time. The

bold blue line near the apex of the dip is a polynomial fit to the peak. The roots of this polynomial are to monitor the peak position with high (0.1 nm) precision with a 1s acquisition time.

An important issue in SPRS is the acquisition of an accurate spectral power reference. For various reasons, this is best done with P-polarized light. But, in order to use P-polarized light to collect a reference, i.e. a spectrum without a resonance feature for reference, it is necessary to change the refractive index of the system dramatically so that there is no SP resonance in the wavelength or angle range of interest. This is simply done by using a dry (N_2 filled) cell. For this reason a P-polarized spectral power reference is taken at this point on the clean, dry Au film.

The next step involves acquisition of a reference spectrum that has a surface plasmon absorption to establish a baseline from which shifts in the SPR angle and wavelength can be measured. For this spectrum a pure solvent is delivered to the flow cell, and the SPR reflection spectrum is recorded.

Figure 3. Resonance between photons of light and plasmons is seen in a graph of reflectivity versus wavelength. Blue line is a polynomial fit used to precisely determine the peak wavelength.

Figure 3. Reflectivity versus wavelength (nm)

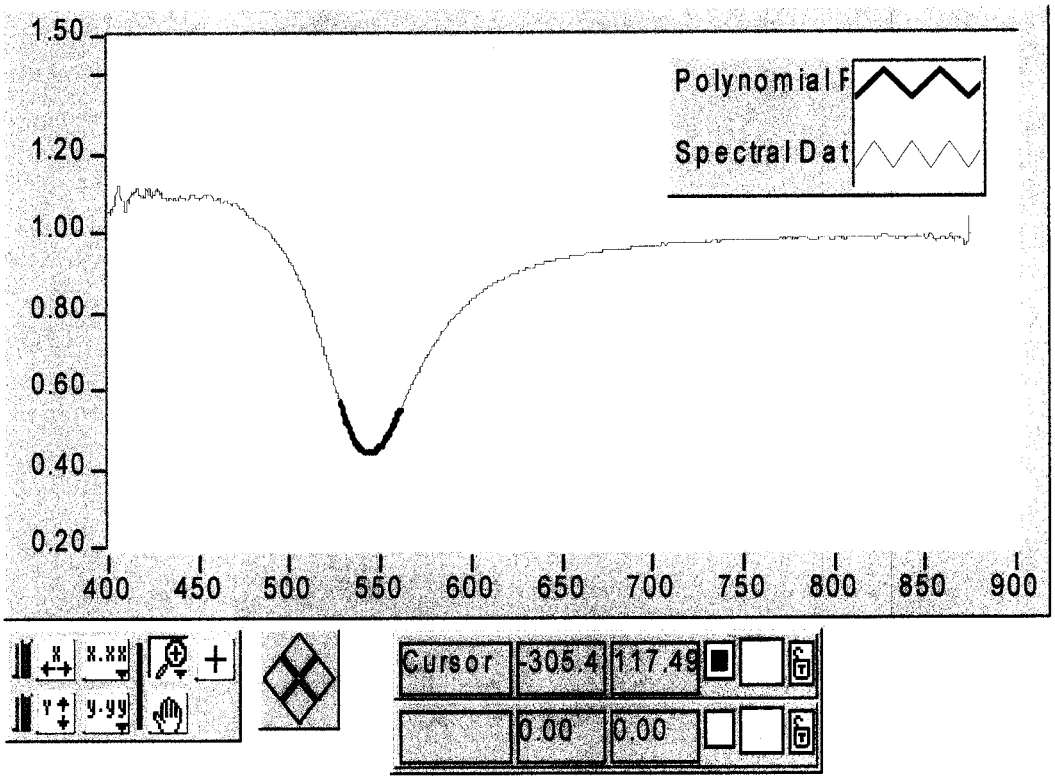

The choice of solvent depends on the experiment, but generally we use the pure solvent without analyte as a reference, e.g. acetone in the case of MgPc studies. Water was used to as a reference system to look at dispersion in acetone, acetonitrile and toluene.

9.8 Angle and Wavelength Modulation

The data that we desire consists of reflectivity as a function of both angle and wavelength. To acquire these data, we wrote a computer program in LabView that takes $R(\lambda)$ spectra at a series of pre-programmed angles. The raw data display from this program is illustrated in **Figure 4**. Please note that in these figures, data points are sequentially numbered and do not correspond to actual wavelengths and angles. The reflectivity axis is accurate. Figure 4 shows reflectivity data for acetonitrile. The positive going peak is actually an inverted representation of the SP resonance in the spectral power reference.

Figure 4. Surface plasmon resonance spectra for 50 sequential angles between 55 and 65 degrees. In the top panel reflectivity is plotted versus wavelength in instrument units. In the bottom panel reflectivity is encoded by color (white is high reflectivity and blue is low) and plotted versus wavelength and angle (3-D $R(\lambda,\theta)$) again in instrument-specific units.

Figure 4. Reflectivity versus wavelength and angle (instrumental units)

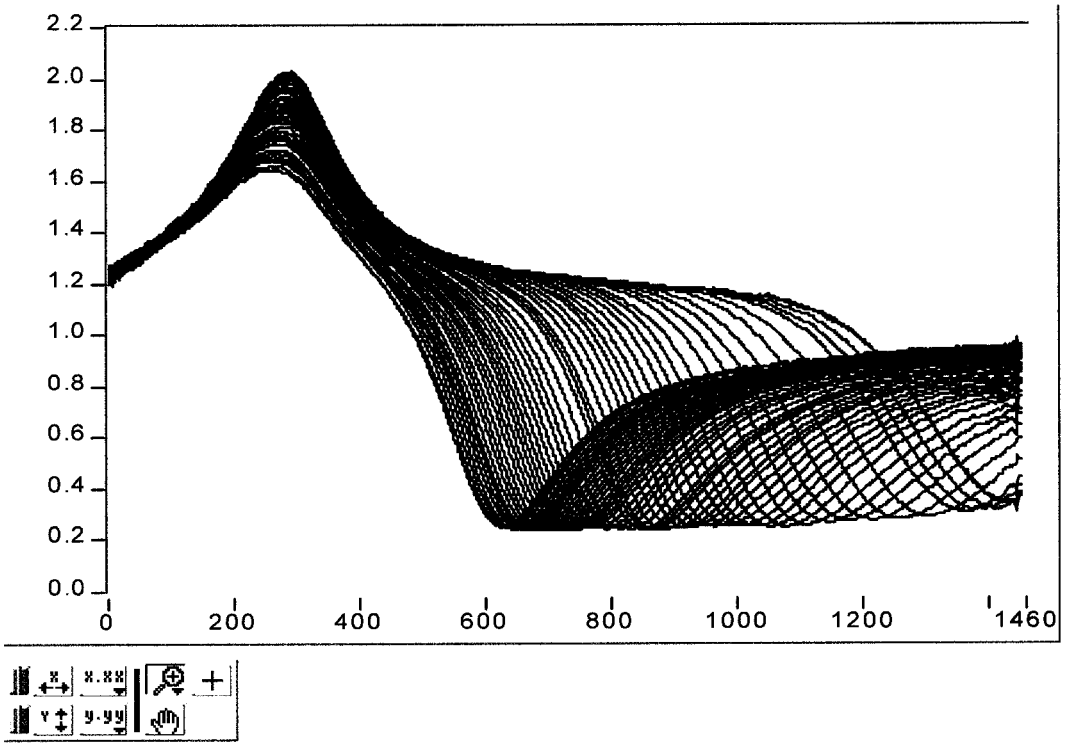

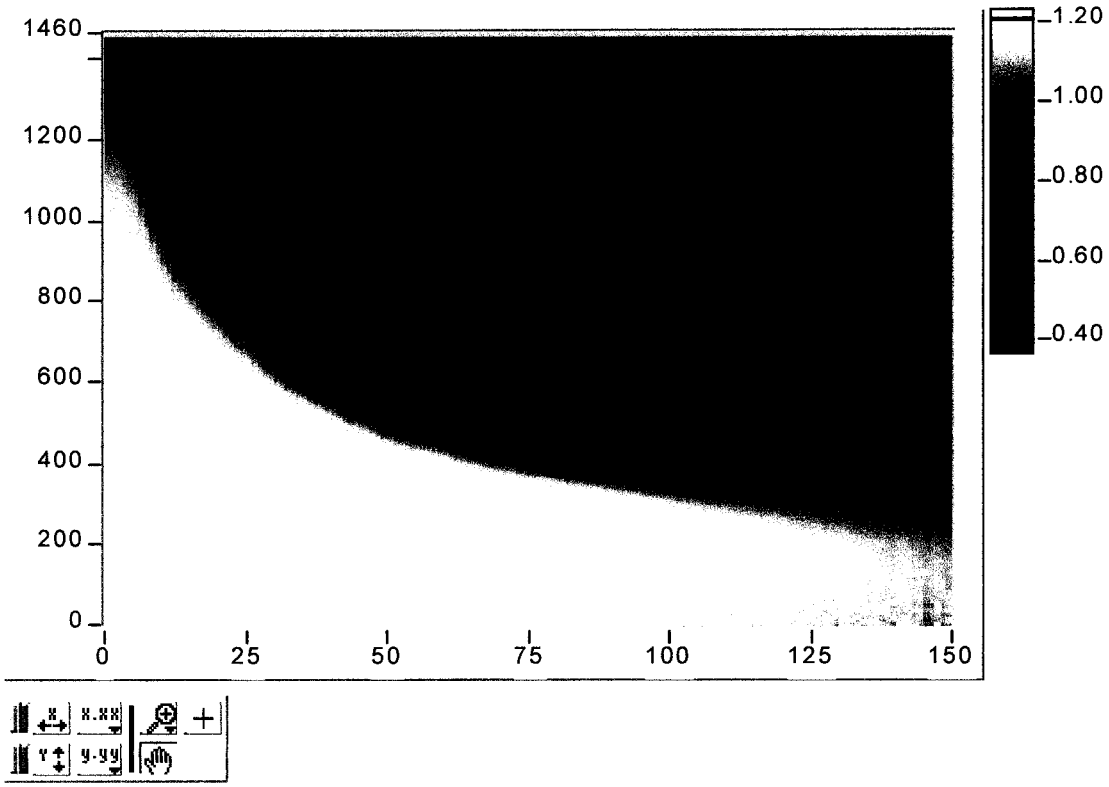

In some cases we wanted to reduce the 3-D $R(\lambda,\theta)$ data into a simpler 2-D spectral response. To do this we measured λ_{SPR} at each successive angle and made plots of $\lambda_{SPR}(\theta)$, or, to emphasize changes from a reference phase, e.g. between water and acetonitrile for example, we would collect $\lambda_{SPR}(\theta)$ for water and then for acetonitrile and then plot the difference as $\Delta\lambda_{SPR}(\theta)$. The θ abscissa is not particularly helpful however when comparing SPR data to reference data on refractive index dispersion. Accordingly, the $\Delta\lambda_{SPR}$ values are graphed in **Figures 5a** versus the original λ_{SPR} values ($\Delta\lambda_{SPR}(\lambda_{SPR})$). Fresnel simulations suggest that a graph of reflectivity difference taken from the $R(\lambda,\theta)$ surface along the apex of the SPR absorption band should be characteristic of RI dispersion in the analyte as well, but these data proved highly irreproducible for reasons that are unclear at the moment **(Figure 5b)**.

Figure 5. 2-D spectral response derived from 3-D $R(\lambda,\theta)$ plots for transparent analytes.

A. Changes in λ_{SPR} versus λ_{SPR} . **B**. Changes in R_{SPR} versus λ_{SPR} .

Figure 5a. $\Delta\lambda_{SPR}(\lambda_{SPR})$ shift data analysis for transparent analytes

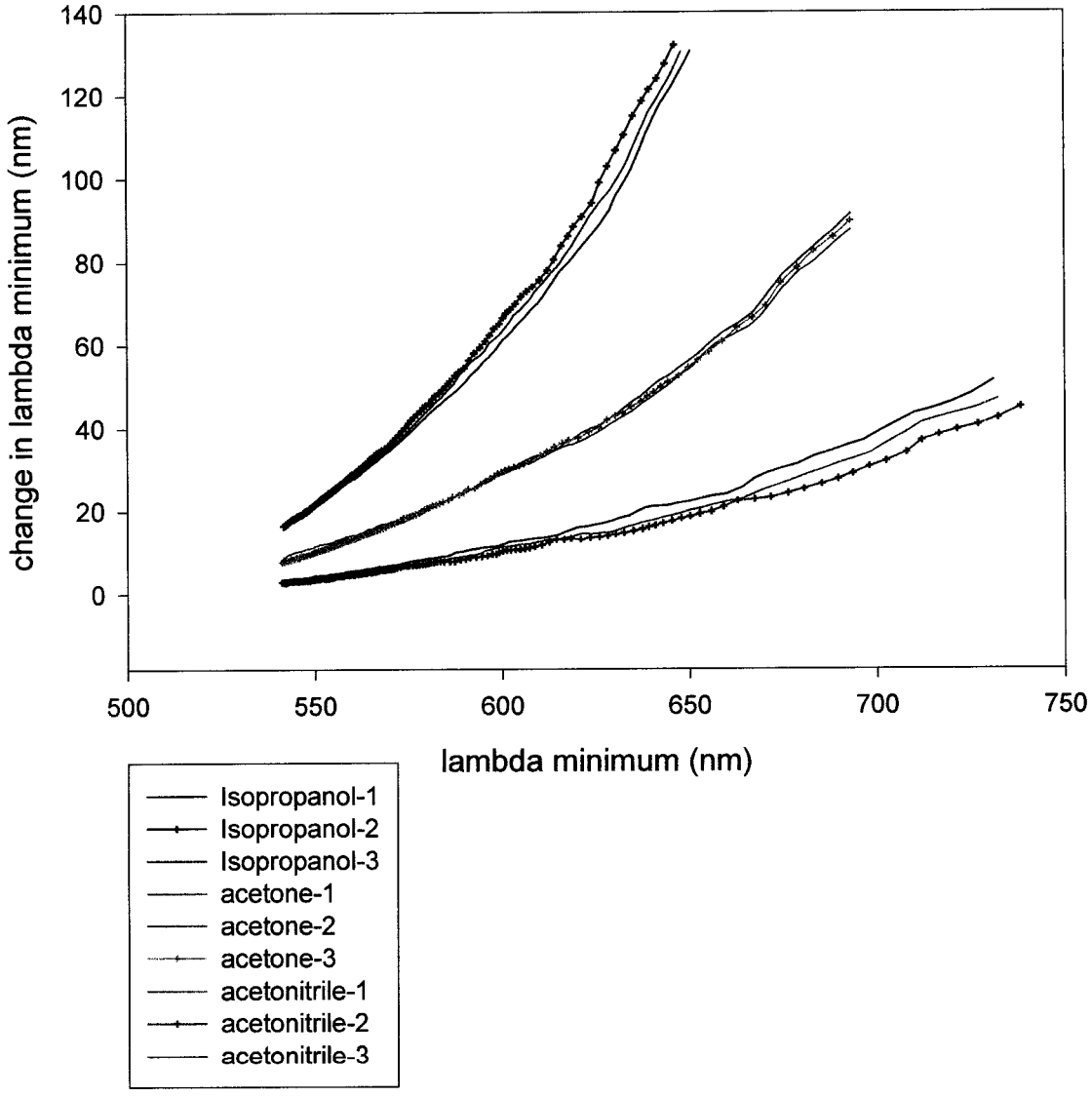

Figure 5b. $\Delta R_{SPR}(\lambda_{SPR})$ data analysis for transparent analytes

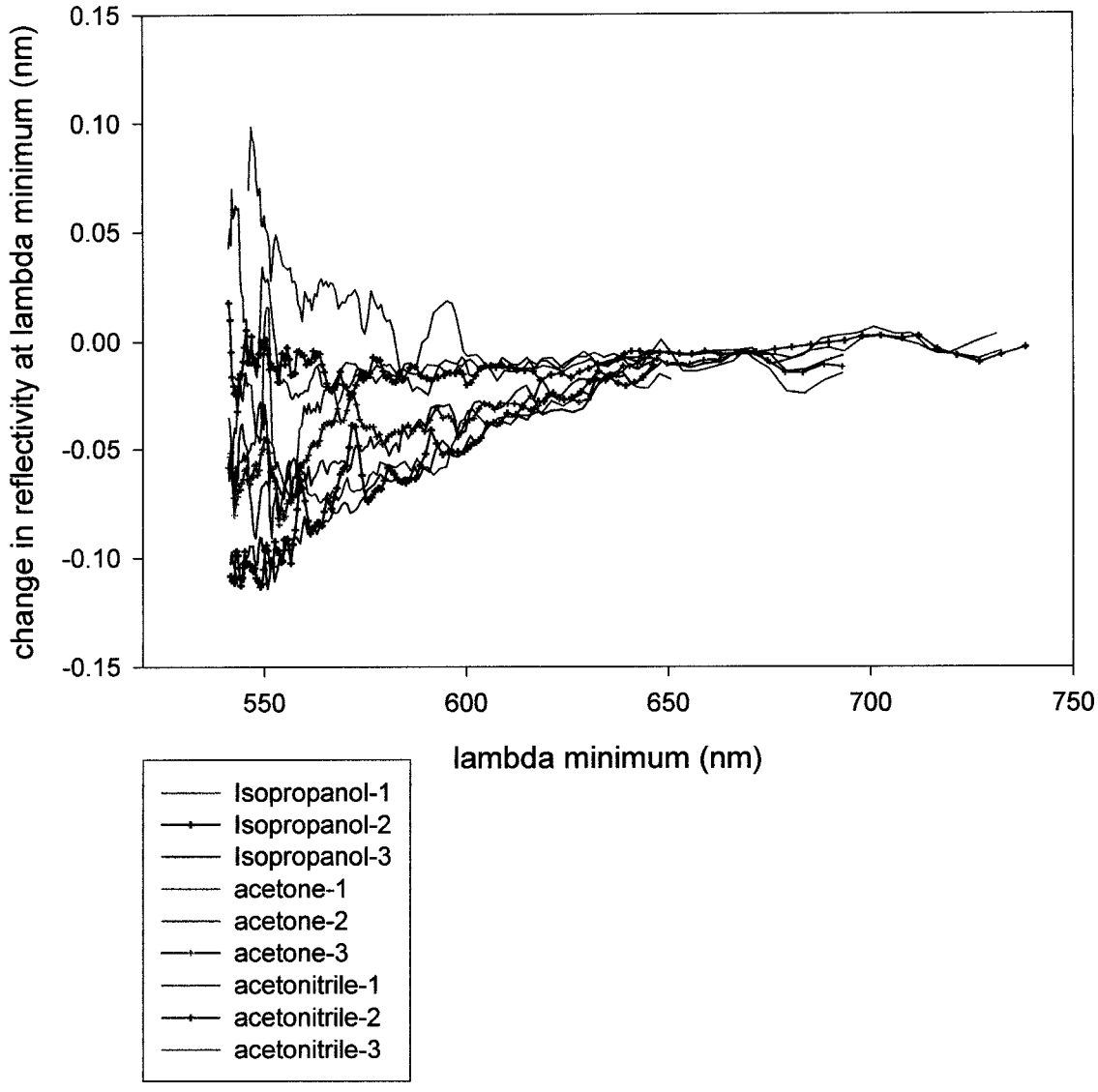

9.9 Limitations related to choice of a colored analyte.

Our group was interested in finding a molecule that would satisfy the following criteria: solubility in an appropriate solvent, significant adsorption to clean gold, a high extinction coefficient, a narrow absorption band, and a λ_{MAX} value within our spectrometer's capabilities. Since our system utilizes white light from a tungsten halogen source, it emits primarily in the visible and near infrared region of the spectrum. The SP resonance on gold is observed at $\lambda \geq 550$nm (SP frequencies never exceed the plasma frequency of the metal) and our spectrometer is limited to $\lambda \leq 900$nm, so model analytes that absorb well within this region were needed. Of numerous candidates explored, including chlorophyll, copper phthalocyanine tetrasulfonic acid, bromothymol blue and others, the one dye that met these criteria was magnesium phthalocyanine (MgPc). MgPc λ_{MAX} is at 670 nm, exceeds 10^5 liters mol^{-1} cm^{-1}, and is unusually sharp ($\approx$25 nm FWHM). MgPC solubility is very limited but is adequate in acetone.

10.0 Results and Discussion

10.1 Introduction

A typical SPR scan consists of reflectivity versus angle R(θ) or wavelength R(λ). Karlsen et al. (10) have referred to this as zeroth-order sensors because SPR spectra are reduced to a single data point (λ_{SPR} or θ_{SPR}). In contrast, a first-order SPR sensor produces a spectral response. The Karlsen first order SPR sensor is a "lightpipe" configuration that internally reflects white light in a glass microscope slide coated with a 50 nm Au film. When the light exits the slide, it consists of a series of discrete bands, each of which covers a different range of angles. The output is rather complex, but the approach is elegantly simple. Our system is a more straightforward example of a first order SPR sensor. Our instrument simply scans a range of angles and collects reflectivity spectra at each one. This information is collected as R(λ,θ) surfaces that illustrate the curved trajectory of the surface plasmons absorption to near surface absorbers.

There are few reports of R(λ,θ) SPR responses. In the early 1980's, Pockrand and Mobius et al. investigated these responses. These studies highlighted a spectral branching response characteristic of strong absorbers that was also observed in this study. The R(λ,θ) SPR theme was recently examined in a brief report by Karlsen et al. (11). The RI spectrum (n(λ)) and absorbance spectrum (k(λ)) can (in theory) be collected together by analysis of the R(λ,θ) surface. We demonstrate this in the visible wavelength range. The present study can be thought of as SPR coupled attenuated total reflection (ATR) spectroscopy. We hope to add qualitative spectral information to the quantitative SPR shift information.

10.2 Analysis of reflectivity surfaces for transparent analytes

An expansion of the conventional reflectivity experiment is illustrated as a contour plot in **Figure 6**, red indicating high reflectivity and black low. In this figure, 150 spectral scans taken in turn at angles between 55 and 70 degrees on a 0.1° interval. The blue-black curved swath that cuts from upper left to lower right of the surface illustrates the absorption of incident light by plasma resonance. The qualitative aspects of this curve are described by the following equations (1-6) derived from the oft-cited review by Knoll et al. (4). The high frequency (ca. 550 nm) asymptote of this curve is a function of the plasma frequency of the metal:

1. $$\omega_{MAX} = \frac{\omega_P}{\sqrt{1+\varepsilon_D}}$$

where ω_{MAX} is the maximum frequency of the surface plasmon, ω_P is the plasma frequency of the metal and ε_D is the dielectric constant of the phase in contact with the metal. The low frequency asymptote arises because of the dependence of the in-plane component of the **k**-vector of the surface plasmon, $\mathbf{k}_{SP}$, on the dielectric constant of the metal, ε_M. At lower frequencies, ε_M increases, so the surface plasmon wave vector, k_{SP}, given by:

2. $$k_{SP} = \frac{\omega}{c}\sqrt{\frac{\varepsilon_M \varepsilon_D}{\varepsilon_M + \varepsilon_D}}$$

begins to approach that of the incident light:

3. $$k_{PH} = \frac{\omega}{c}\sqrt{\varepsilon_D}$$

Figure 6. Reflectivity is plotted in false color (red = high reflectivity, blue = low) as a function of angle and wavelength illustrating the curved trajectory of the surface plasmon absorption band (blue curve) when viewed in this space. The red band on the lower left is an artifact of a plasmon resonance in the spectral power reference (N_2-filled cell). The hemispherical optic is sapphire coated with chromium (1 nm), gold (50 nm) and is contacting acetone.

Figure 6. Contour Plot

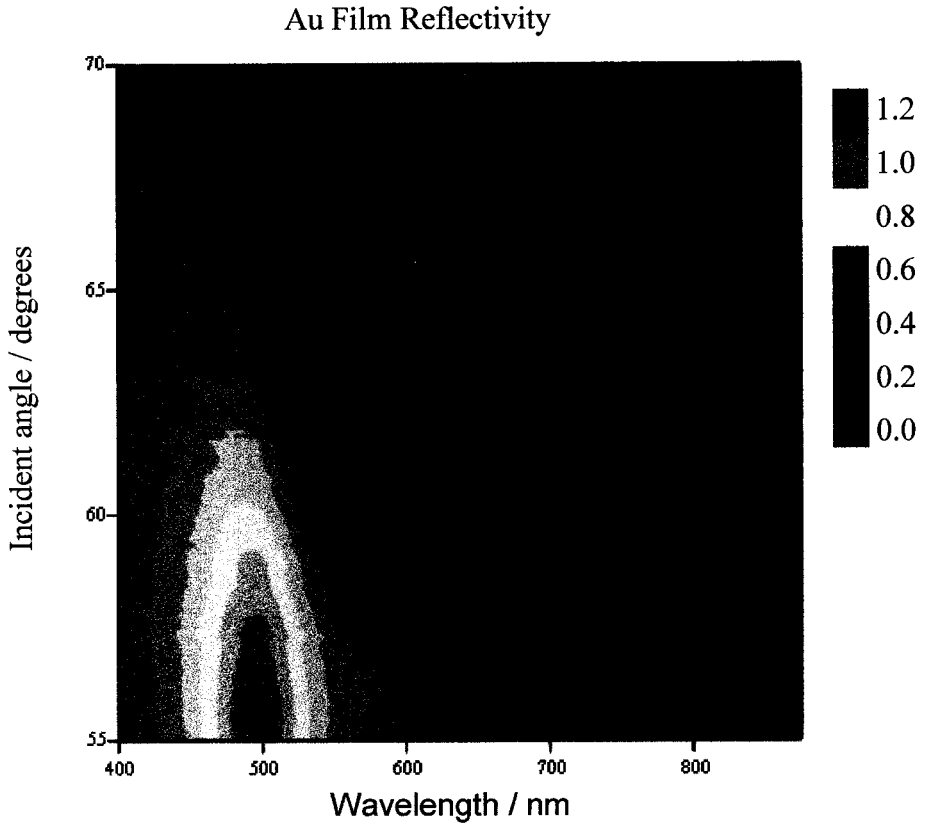

The practical consequence of the latter is that at lower angle (longer wavelength) the conditions needed to excite the surface plasmon begin to depend less on light frequency when $\varepsilon_M(\lambda) > \varepsilon_D(\lambda)$, and more on incident angle through the relationship:

4. $$k_{PH} = \frac{\omega}{c}\sqrt{\varepsilon_D}\sin(\theta)$$

From an analytical perspective, this means that for a given displacement of this curve, due to a change in surface RI, the corresponding changes in λ_{SPR} and θ_{SPR} will be of different magnitude at different points. This is further illustrated in **Figure 7A**, where only those (θ,λ) points that correspond to the apex of the surface plasmon absorbance are plotted for water (n=1.33, lower curves) and acetone (n=1.36, upper) respectively. This λ_{SPR} vs θ_{SPR} curve is formally related to the well-known ω-k dispersion curve through the following:

5. $$\omega_{SP} = \frac{2\pi c}{\lambda_{PH}}$$

and

6. $$k_{SP} = \frac{2\pi}{\lambda''} = \frac{2\pi n_P \sin(\theta)}{\lambda_{PH}}$$

7. $$k_{SP} = \frac{\omega}{c}\sqrt{\frac{\varepsilon_M \varepsilon_D}{\varepsilon_M + \varepsilon_D}}$$

where ω_{SP} is the surface plasmon frequency, λ_{PH} is the photon vacuum wavelength, n_P is the prism refractive index and θ is the angle of incidence. When equations 6 and 7 are equal to each other then resonance occurs.

The conventional SPR measurement employs either fixed λ and measures $\Delta\theta$, or vice-versa yielding $\Delta n_{SURFACE}$ from $\Delta\lambda$ or $\Delta\theta$ shifts illustrated by the horizontal and vertical arrows in Figure 7A, respectively. Figures 7B and 7C illustrate the magnitudes of the $\Delta\lambda(\theta)$ and $\Delta\theta(\lambda)$ functions respectively for the given change in refractive index $\Delta n \approx (1.33 \rightarrow 1.36)$. The 8B and 8C curves are a spectral response that at each wavelength it is proportional to $\Delta n(\lambda)$. The solid lines are Fresnel simulations that employ the n_D^{20} values of the refractive index of water and acetone respectively – ignoring the slight RI dispersion for these transparent solvents. It is clear that the sensitivity of $\Delta\lambda$ and $\Delta\theta$ responses are larger at lower θ and λ respectively. The small spectral mismatch between the Fresnel simulation and the data likely reflects a small RI dispersion. RI dispersion is a potential avenue to pursue spectral selectivity. But for transparent analytes this dispersion is probably too small to be a useful spectral signature, especially for studies of interfacial binding where adsorbate contributions to interfacial RI are already small. The benefit of an added spectral dimension was pointed out by Georgiadis et al. (18) for determining both RI and thickness of thin adsorbed layers, referred to as multicolor SPR, but this specific issue was not addressed in this work.

Figure 7. Plots derived from reflectivity data like those in Fig. 3 but containing only those points corresponding to the apex of the SPR absorption band in the angle-wavelength plane. **A**. SPR peak absorption wavelength as a function of incident angle for water (n=1.33, lower curves) and acetone (n=1.36, upper curves). **B**. Resulting shift in wavelength as a function of angle ($\Delta\lambda_{SPR}(\theta)$) showing larger sensitivity at lower angle (and longer wavelength). **C**. Shift in angle as a function of wavelength ($\Delta\theta_{SPR}(\lambda)$) showing a modest decrease in sensitivity at longer wavelengths (lower angle).

Figure 7. An example of a transparent analyte: acetone

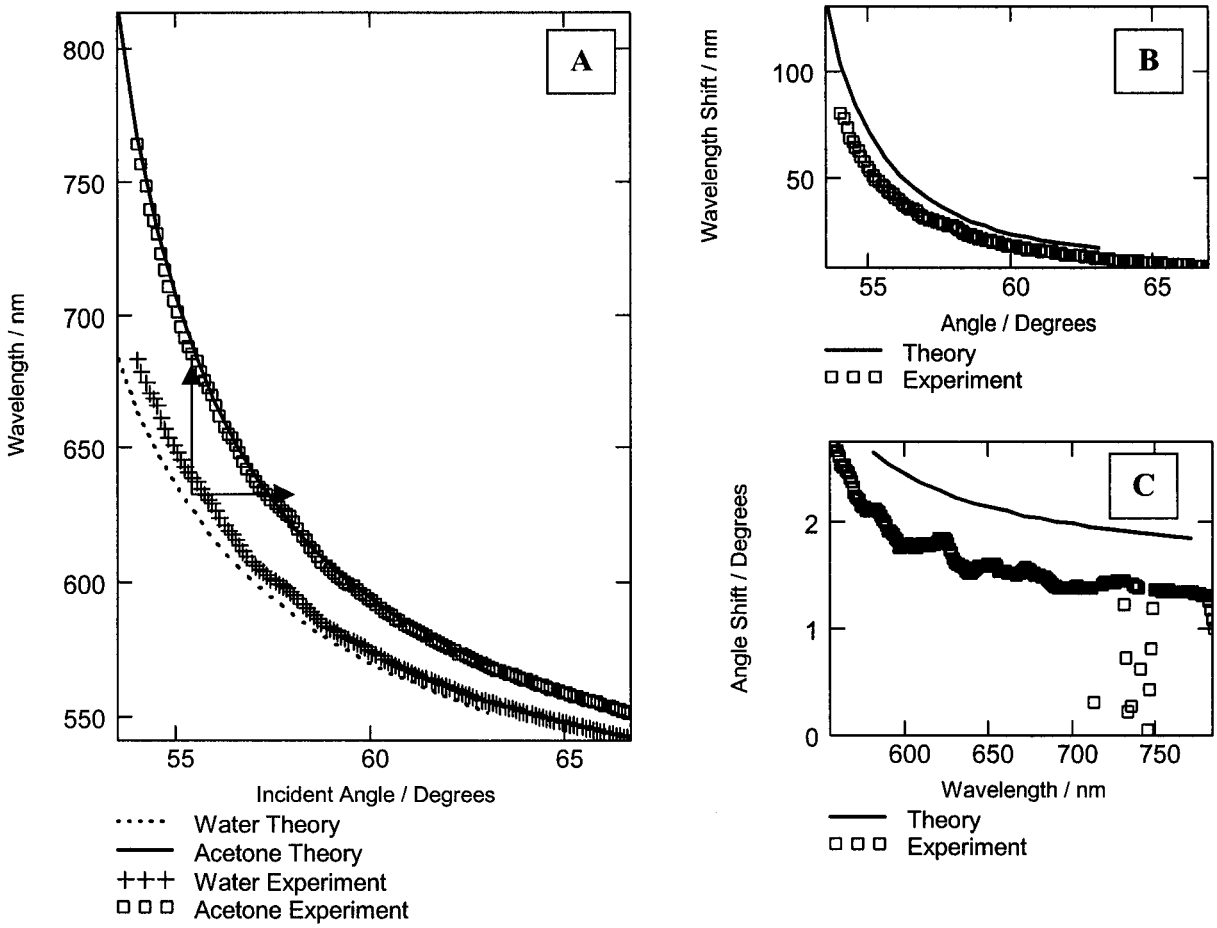

10.3 Analysis of reflectivity surfaces for absorbing analytes

Absorption bands are derived from oscillations in N(λ) that should produce distinctive signatures in the λ-dependent SPR spectra. In the following section Fresnel simulations and experimental measurements of the SPR spectra of adsorbed MgPc are shown. The Fresnel simulations require knowledge of the wavelength dependent complex refractive index function N(λ) for all of the relevant phases involved in the reflection. N(λ) for the solution phase may be derived from standards as follows: The absorbance of a phase determines the complex refractive index, k:

6. $$k(\lambda) = \frac{2.303\, A(\lambda)\lambda}{4\pi b}$$

where A is the absorbance and b is the path length. Hence absorption bands are oscillations in k. Oscillations in k in turn produce oscillations in n because n is the Kramers-Kronig transform of k. So, measurement of an absorption spectrum gives sufficient information to compute the wavelength dependent complex refractive index

7. $$N(\lambda) = n(\lambda) + ik(\lambda)$$

n(λ) is derived from k(λ) using as serial Fourier transform method outlined by Bertie (42).

These complex RI data were used to model experimental data and the results are plotted in Figure 9. For computational efficiency a Drude-Lorenz function that directly yields the complex dielectric function ε(λ) was used in place of the KKT-derived optical constants of MgPc. This allowed the concentration of the MgPc layer to be a single adjustable parameter when matching experiment and theory. Contrary to initial

expectation, adequate simulation of these spectra required that the MgPc be concentrated into a compact adsorbed layer on the Au surface that is 1 nm thick and ≈ 0.6 M in concentration – reasonable values for an assumed adsorbed layer. Sequential panels in **Figure 9** portray reflectivity spectra for a series of increasing incident angles. As the incident angle increases, the surface plasmon band blue-shifts (as expected), moves toward the MgPc band, mixes with it, and continues. The mixing is somewhat unusual because rather than simply merging with the MgPc dip (as one might expect for absorption peaks) and then moving further to the blue, the SPR dip appears to stop about 20 nm short of the MgPc dip and then slowly diminish in intensity. Just as the 'SPR' dip is arrested, the 'MgPc' dip begins to intensify and blue shift, taking on as it were the identity of the SPR dip. When peak wavelengths are plotted versus incident angle, the resulting curve branches near λ_{MAX}(MgPc). The SPR branch is arrested at a just greater than λ_{MAX}(MgPc), and the former MgPc branch intensifies and begins to shift in the expected trajectory of the SPR dip. This behavior was first predicted by Pockrand et al. (43) and then later observed by Mobius et al. (44) in studies of Langmuir-Blodgett dye layers on Ag. Branching is reproduced in Fresnel simulation (solid line) only when a thin (e.g. 1-3 nm) layer of very concentrated MgPc is assumed to exist on the surface of the gold – an indication of MgPc adsorption seen in Figure 10. The branching phenomenon is reproduced for a limited set of conditions. For most absorbing layers, specifically ones with weaker absorption, or thicker and weaker ones, oscillations in $N(\lambda)$ result in linear oscillations in $\lambda_{SPR}(\theta)$ and $\theta_{SPR}(\lambda)$ (27).

Figure 8. Imaginary (k, solid line) and real (n, dashed line) refractive index (RI) spectra of 1 μM magnesium phthalocyanine in acetone. Real RI (n) data are the Kramers-Kronig transform of k. For n, only oscillations are shown, and the average value (1.36) is subtracted out.

Figure 8. Magnesium phthalocyanine in acetone

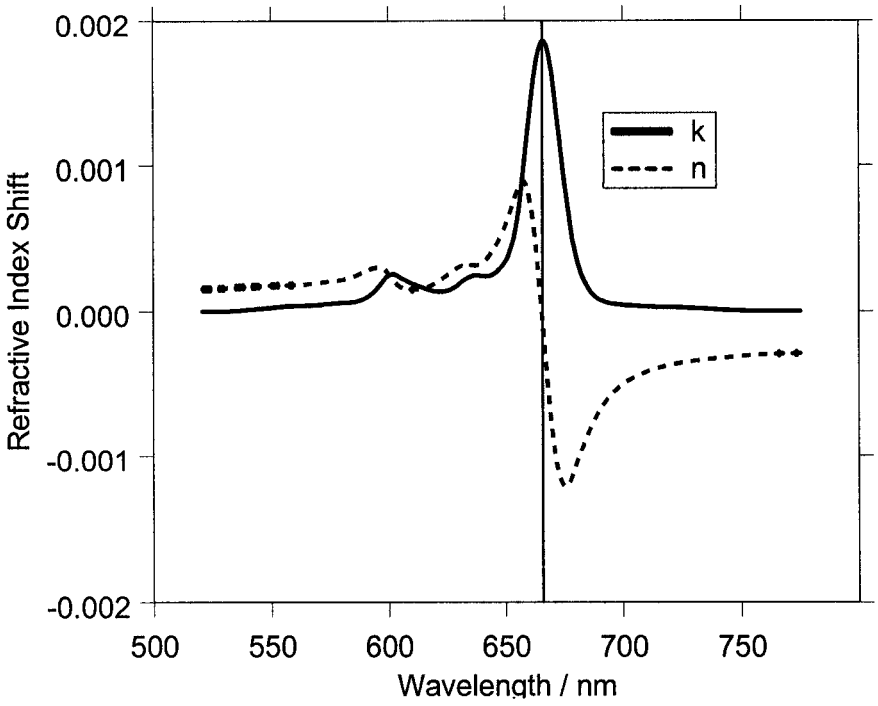

Figure 9. Fresnel simulations (dashed lines, sapphire | Au (50 nm) | MgPc (1 nm) | acetone) and experimental (solid lines) reflectivity spectra recorded over a progression of increasing angles. The vertical line corresponds to the peak absorption wavelength of the Magnesium phthalocyanine-acetone solution. As the angle increases the SPR peak blue-shifts, but never coincides exactly with the Mg phthalocyanine absorption.

Figure 9. Fresnel-simulated and experimental reflectivity versus wavelength

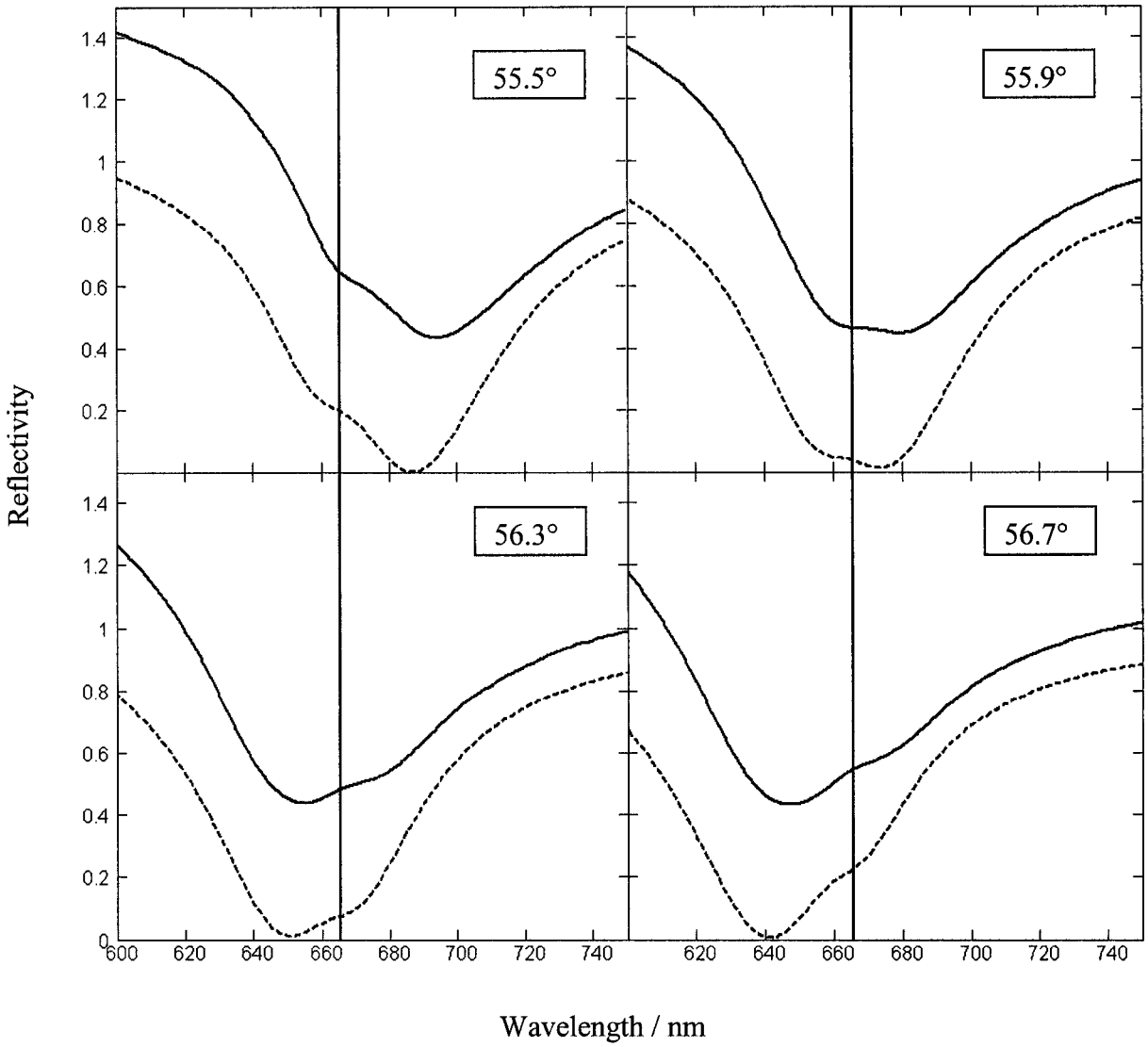

Figure 10. Wavelength of the absorptive dips appearing in the Fresnel simulated (solid lines, for the sapphire | Au (50 nm) | MgPc (1 nm) | acetone) and experimental (symbols) reflectivity spectra as a function of incident angle. At a given angle, two dips may be present – one for MgPc and one for SPR. As the angle is scanned, the SPR dip follows the trajectory characteristic of the surface plasmon resonance, and the other (MgPc) remains stationary. But carefully following each peak reveals the branching phenomenon as indicated. The red-shifting SPR dip is arrested at the MgPc wavelength, and the erstwhile MgPc dip begins to red-shift instead. The dashed vertical line indicates the peak absorption wavelength of the magnesium phthalocyanine solution.

Figure 10. θ_{SPR} versus λ illustrating spectral branching

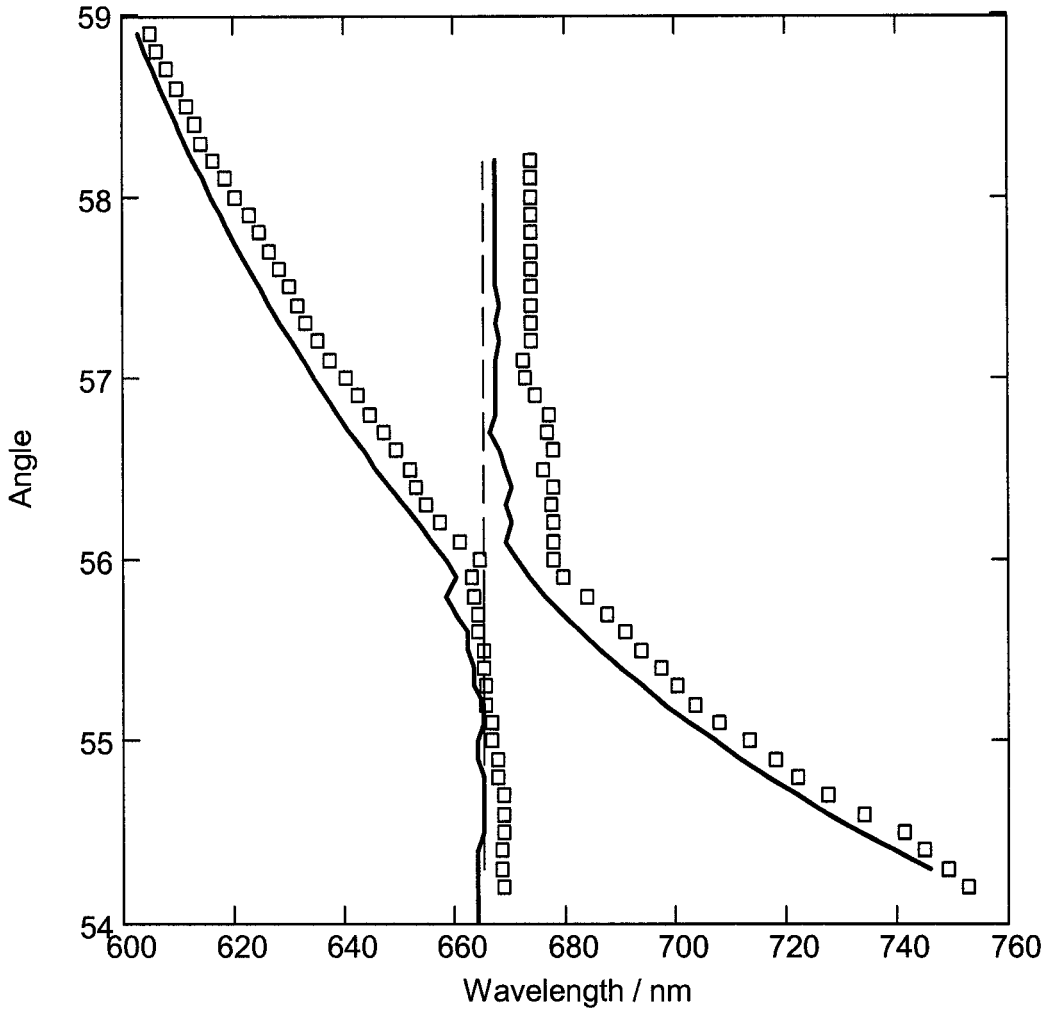

In **Figure 11A**, the MgPc k-spectrum is shown atop a Fresnel simulation of the reflectivity surface $R(\lambda,\theta)$. The coupling between the SPR spectrum and the absorption band is seen as a deviation in the SPR band where it coincides with the MgPc λ_{MAX}. Plotting $\Delta R(\lambda,\theta)$, the difference in reflectivity between the MgPc simulation and a blank acetone one, is even more helpful **(Figure 11B)**. This presentation of the data shows a differential reflectivity response in the four areas (crudely quadrants) delineated by the two black reference lines. Low reflectivity appears on the upper right and lower left, and high reflectivity in the upper left and lower right quadrants. The experimental data (**Figure 11C**) are largely in agreement with theory but show a considerably diminished absorption on the upper right. The spectral detail derived from MgPc through scanning λ_{SPR} can be compared to that derived from an ATR experiment. **Figure 12** shows a calculated MgPc ATR difference reflectivity spectrum (solid line) alongside the corresponding experimental and theoretical $\Delta R_{SPR}(\lambda)$ data. The two simulated difference spectra differ in just two ways. The SPR spectra are simulated for:
sapphire | Au(50 nm) | MgPc (1 nm) | acetone layers at 57.5°; the ATR spectra are calculated for the same optical configuration minus the Au layer and at the angle (50.6°) that maximizes the absorption. The reference spectrum in all cases is pure acetone. Clearly the surface plasmon complicates the spectral response viewed in this way. On the other hand, the surface plasmon coupled spectrum is highly responsive to both the real and imaginary parts of the MgPc spectrum, and thus provides a signature for both absorbing and transparent adsorbates.

Figure 11. Theoretical (**A,B**) and experimental (**C**) reflectivity surfaces. Blue indicates low reflectivity and red high. The experimental **k**-spectrum of MgPc is depicted for reference as a solid blue figure atop panels **A**, **B** and **C**. The vertical line indicates the peak absorption (k) value. Panel **A** is a Fresnel simulation of the reflectivity surface corresponding to the SPR coupled ATR spectrum of Mg phthalocyanine. Panels **B** and **C** are Fresnel simulation and experimental *difference* reflectivity surfaces respectively. Difference reflectivity is defined as R_{MgPc} - $R_{Acetone}$ where acetone serves as a blank. The black curves superimposed on panels **A-C** indicate the position of the surface plasmon dip for the blank acetone scan.

Figure 11. Difference Reflectivity

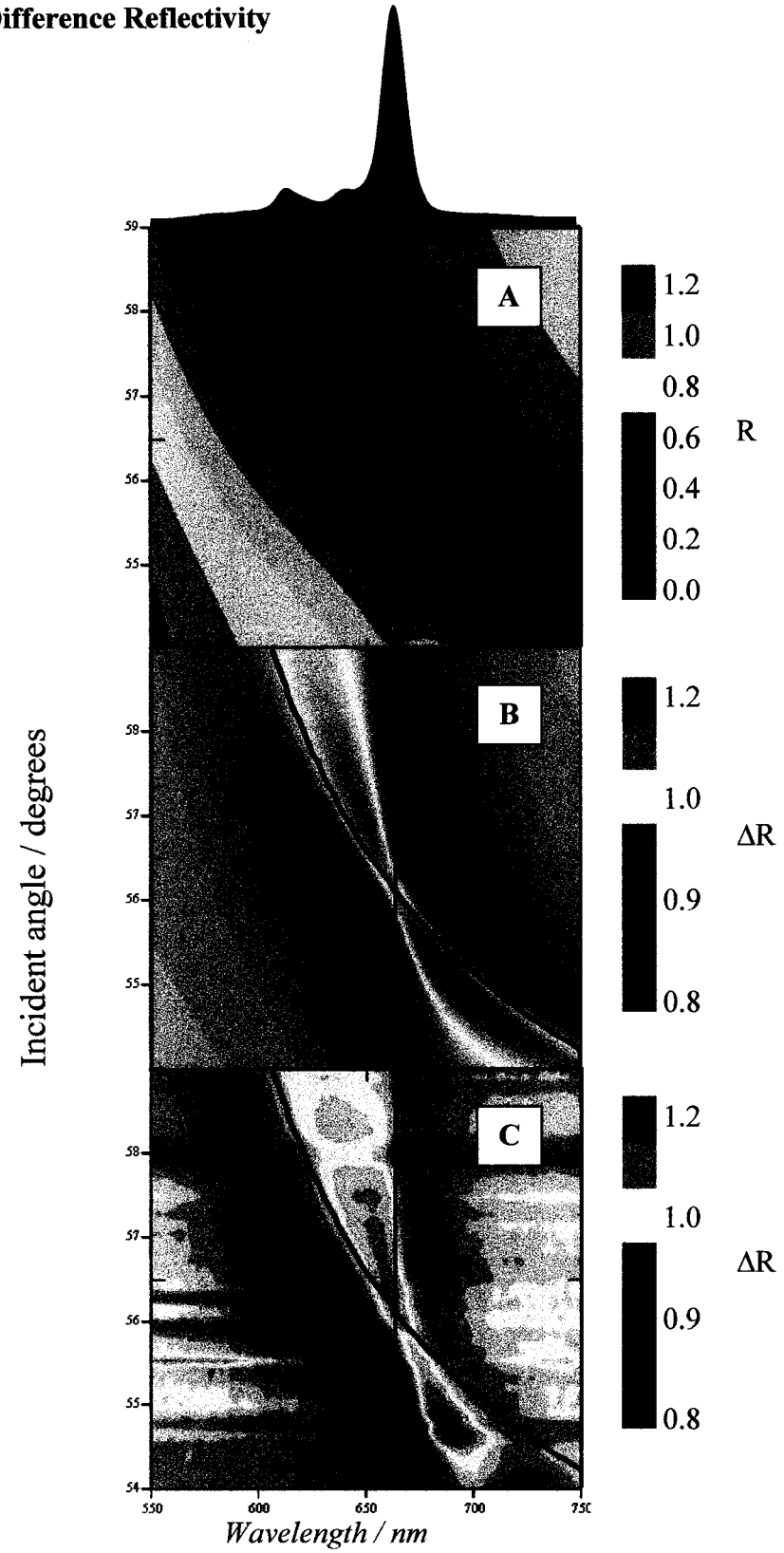

Figure 12. Theoretical and experimental P-polarized difference reflectivity spectra of a 1 nm MgPc layer either at the sapphire-acetone interface (conventional ATR spectrum, solid line), or at the Au-acetone interface in an SPR coupled setting (short dashes are Fresnel simulation for 56.5°, long dashes are experiment). Simulated ATR spectrum uses $\theta = 50.6°$, maximizing signal.

Figure 12. Attenuated Total Reflection

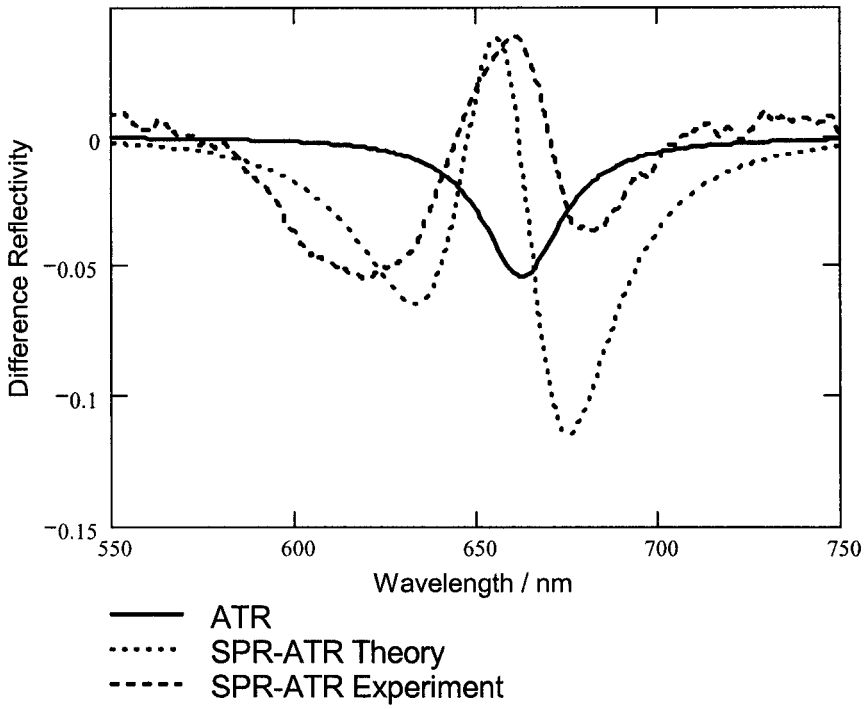

10.4 Comparison to Boussaad et al. work

These experiments may be compared with recent ones reported by Boussaad et al. (28). They utilized a high resolution multiwavelength SPR technique that measured the "electronic state" of a protein, cytochrome C. They reduced and oxidized the heme center in the protein and detected the corresponding change in electronic absorption with an SPR method. Their instrument tracks the angle corresponding to the apex of the SPR dip, the 'SPR angle' or θ_{SPR} during a scan of the incident wavelength. This gives a $\Delta\theta_{SPR}(\lambda_{SPR})$ spectrum that is in direct proportion to the surface RI dispersion spectrum because $\Delta\theta_{SPR}(\lambda_{SPR})$ is a linear function of $\Delta n_{SURFACE}(\lambda)$ (28). The RI dispersion spectrum is clearly characteristic of the near-surface absorber and can be converted to the more familiar absorbance ($k(\lambda)$) spectrum with the Kramers-Kronig transform.

We measure reflection spectra on a CCD spectrometer as a function of incident angle. Taken together these spectra comprise the $R(\lambda,\theta)$ optical response and encode more information, but less precisely in the θ dimension. The $R(\lambda,\theta)$ surface can be used as a fingerprint, or for the extraction of $\lambda_{SPR}(\theta)$ dispersion curves analogous to the $\theta_{SPR}(\lambda)$ measured by Boussaad et al. (28). The $\lambda_{SPR}(\theta)$ dispersion curve for MgPc is unusual because of a branching phenomenon related to the intense absorption band. Attempts to track $\lambda_{SPR}(\theta)$ or $\theta_{SPR}(\lambda)$ is frustrated because $\lambda_{SPR}(\theta)$ is not single-valued and $\theta_{SPR}(\lambda)$ is discontinuous with spectral branching (see Figure 10). In the case of a weaker absorber, theory predicts that oscillations in the reflectivity (R) dimension should reveal $k_{SURFACE}(\lambda)$ directly, and that oscillations in λ_{SPR} reveal $n_{SURFACE}(\lambda)$ directly.

11.0 Conclusion

Experiments with transparent analytes illustrated the curved 'spectral' responses expected from Fresnel theory in the form of $\lambda_{SPR}(\theta)$ or $\theta_{SPR}(\lambda)$ plots where a gradual increase in spectral shift per unit RI is observed as a function of wavelength. These plots serve to show that at least in theory the spectral dispersion in refractive index should be observable using this method. Our modeling results are limited in this area however. The use of single, wavelength independent values for the refractive indexes of acetone and water gave fairly good agreement with theory – a result that suggests that the slight dispersion in refractive index for these solvents is probably not a sufficiently distinctive spectral signature for analytical speciation. In other words, if one were to analyze two different transparent analytes with similar refractive indices they might be indistinguishable.

The second part of the experiment included the investigation of an absorbing dye molecule, magnesium phthalocyanine (MgPc) that did exhibit a significant molecular fingerprint. The anomalous dispersion in refractive index associated with the absorption band of dye was evident in both $\Delta\lambda_{SPR}(\theta)$ and $\Delta R(\lambda,\theta)$ plots, and in good agreement with Fresnel theory. When MgPc data were represented as a 2-D spectrum of resonance wavelength versus incident angle, the effects of SPR and MgPc-based spectral peak mixing led to spectral branching that needed fairly careful attention to analyze.

12.0 Future Work

Current work suggests that we explore near infrared (NIR) wavelengths in the future. Nearly all analytes exhibit distinctive NIR vibrational overtone absorption spectra and the optical constants of Au and Ag are appropriate in the NIR region for SPRS spectroscopy. As a practical point, we believe that investigations of biochemical problems would be suitable analytes of interest given the need for accurate and selective bioanalyses. Since most of the SPRS studies are biochemical in nature and utilize BIAcore instruments that scan angles at a fixed wavelength, incorporating the angle and wavelength modulated system may provide more information for biochemical problems. Simple model systems such as biotin-streptavidin interactions can first be analyzed before investigating more complex biochemical interactions with this SPR system.

REFERENCES

1. Homola, J.; Yee, S.S.; Gauglitz, G. *Sensors and Actuators B,* **1999**, *54*, 3-15.

2. Green, R.J.; Frazier, R.A.; Shakesheff, K.M.; Davies, M.C.; Roberts, C.J.; Tendler, S.J.B. *Biomaterials,* **2000**, *21,* 1823-1835.

3. See any physics book

4. Knoll, W. *Annu. Rev. Phys. Chem.* **1998**, *49*, 569-638.

5. Zhu, X. -M.; Lin, P. -H.; Ao, P.; Sorenson, L.B. *Sensors and Actuators B*, **2002**, *84,* 106-112.

6. Lu, H.B.; Homola, J.; Campbell, C.T.; Nenninger, G.G.; Yee, S.S.; Rather, B.D. *Sensors and Actuators B,* **2001**, *74*, 91-99.

7. Nelson, R.W.; Nedelkov, D.; Tubbs, K.A. *Anal. Chem.* **2000**, 404A-411A.

8. Nedelkov, D. and Nelson, R.W. *Analytica Chimica Acta*, **2000**, *423*, 1-7.

9. Brockman, J.M.; Nelson, B.P.; Corn, R.M. *Annu. Rev. Phys. Chem.* **2000**, *51*, 41-63.

10. Karlsen, S.R.; Johnston, K.S.; Yee, S.S.; Jung, C.C. *Sensors and Actuators B*, **1996**, *32*, 137-141.

11. Karlsen, S.R.; Johnston, K.S.; Jorgenson, R.C.; Yee, S.S. *Sensors and Actuators B*, **1995**, *24-25*, 747-749.

12. Bailey, L.E.; Kambhampati, D.; Kanazawa, K.K.; Knoll, W.; Frank, C.W. *Langmuir*, **2002**, *18*, 479-489.

13. Zubritsky, Elizabeth. *Anal.Chem.* **2000**, 289A-292A.

14. Xinglong, Y.; Dingxin, W.; Zibo, Y. *Sensors and Actuators*, **2003**, in press

15. Nelson, S.G.; Johnston, K.S.; Yee, S.S. *Sensors and Actuators B*, **1996**, *35-36*, 187-191.

16. Jung, L.S.; Campbell, C.T.; Chinowsky, T.M.; Mar, M.N.; Yee, S.S. *Langmuir*, **1998**, *14*, 5636-5648.

17. Sjolander, S.; Urbaniczky, C. *Anal.Chem.* **1991**, *63*, 2338-2345.

18. Peterlinz, K.A. and Georgiadis, R. *Optics Communications*, 1996, *130*, 260-266.

19. Peterlinz, K.A. and Georgiadis, R. *Langmuir*, **1996**, *12*, 4731-4740.

20. Ehler, T.T.; Malmberg, N.; Noe, L.J. *J. Phys. Chem. B*, **1997**, *101*, 8043.

21. Chinowsky, T.M. and Yee, S.S. *Sensors and Actuators B*, **1998**, *51*, 321-330.

22. Georgiadis, R.; Peterlinz, K.P.; Peterson, A.W. *J. Am. Chem. Soc.* **2000**, *122*, 3166-3173.

23. Sips, R. *J. Chem. Phys.* **1948**, *16*, 490-495.

24. Brennan, C.B.; Sun, L.; Weber, S.G. *Sensors and Actuators B*, **2001**, *72*, 1-10.

25. Iwasaki, Y.; Horiuchi, T.; Niwa, O. *Anal.Chem.* **2001**, *73*, 1595-1598.

26. Baba, A.; Advincula, R.C.; Knoll, W. *J.Phys. Chem. B.* **2002**, *106*, 1581-1587.

27. Kang, X.; Jin, Y.; Cheng, G.; Dong, S. *Langmuir*, **2002**,*18*, 1713-1718.

28. Boussaad, S.; Pean, J.; Tao, N.J. *Anal.Chem.* **2000**, *72*, 222-226.

29. Roy, S.; Kim, J-H.; Kellis, J.T. Jr.; Poulose, A.J.; Robertson, C.R.; Gast, A.P. *Langmuir*, **2002**, *18*, 6319-6323.

30. Westphal, P. and Bornmann, A. *Sensors and Actuators B*, **2002**, *84*, 278-282.

31. Nikitin, P.I.; Grigorenko, A.N.; Beloglazov, A.A.; Valeiko, M.V.; Savchuk, A.I.; Savchuk, O.A.; Steiner, G.; Kuhne, C.; Huebner, A.; Salzer, R. *Sensors and Actuators,* **2000**, *85*, 189-193.

32. Nikitin, P.I.; Beloglazov, A.A.; Valeiko, M.V.; Creighton, J.A.; Smith, A.M.; Sommerdijk, N.A.J.M.; Wright, J.D. *Sensors and Actuators B*, **1997**, *38-39*, 53-57.

33. Haes, A.J. and VanDuyne, R.P. *J. Am. Chem. Soc.* **2002**, *124*, 10596-10604.

34. Malinsky, M.D.; Kelly, K.L.; Schatz, G.C.; VanDuyne, R.P. *J. Am. Chem. Soc.* **2001**, *123*, 1471-1482.

35. VanGent, J.; Lambeck, P.V.; Kreuwel, H.J.M.; Gerritsma, G.J.; Sudholter, E.J.R.; Reinhoudt, D.N.; Popma, Th.J.A. *Sensors and Actuators,* **1989**, *17*, 297-305.

36. Liedberg, B.; Nylander, C.; Lunstrom, I. *Sensors and Actuators* **1983**, *4*, 299-304.

37. Daniels, P.B.; Deacon, J.K.; Eddowes, M.J.; Pedley, D.G. *Sensors and Actuators* **1988**, *15*, 11-18.

38. Spinke, J.; Liley, M.; Guder, H.-J.; Angermaier, L.; Knoll, W. *Langmuir*, **1993**, *9*, 1821-1825.

39. Sigal, G.B.; Bamdad, c.; Barberis, A.; Strominger, J.; Whitesides, G.M. *Anal. Chem.*, 1996, *68*, 490-497.

40. Ostuni, E.; Yan, L.; Whitesides, G.M. *Colloids and Surfaces B: Biointerfaces*, **1999**, *15*, 3-30.

41. Bohn, P.W. "Laser Applications in Chemistry and Biophysics" Proceedings of the SPIE-International Society for Optical Engineering, 1986.

42. The Kramers Kronig transform is implemented via serial Fourier transforms as outlined in **a**. J.E. Bertie and H.H. Eysel. *Appl. Spectrosc.* **1985**,*39*, 392. **b**. J.E. Bertie; H. Harke; M.K. Ahmed; H.H. Eysel. *Croatica. Chem. Acta* **1988**, *61*, 391. **c**. J.E. Bertie; R. Manji; S.L. Zhang. *Appl. Spectrosc.* **1992**, *46*, 1660.

43. Pockrand, I.; Swalen, J.D.; Gordon II, J.G.; Philpott, M.R. *J. Chem. Phys.* **1979**, *70*, 3401-3408.

44. Pockrand, I.; Brillante, A.; Mobius, D. *J. Chem. Phys.* **1982**, *77*, 6289-6295.